Journal of Computational Physics 425 (2021) 109902

Contents lists available at ScienceDirect

Journal of Computational Physics

www.elsevier.com/locate/jcp

An efficient targeted ENO scheme with local adaptive dissipation for compressible flow simulation

Jun Peng [a,*], Shengping Liu [c], Shiyao Li [a,b,c], Ke Zhang [a,b], Yiqing Shen [a,b]

[a] State Key Laboratory of High Temperature Gas Dynamics, Institute of Mechanics, Chinese Academy of Sciences, Beijing, China
[b] School of Engineering Science, University of Chinese Academy of Sciences, Beijing, China
[c] Institute of Applied Physics and Computational Mathematics, Beijing 100094, China

ARTICLE INFO

Article history:
Received 23 March 2020
Received in revised form 29 September 2020
Accepted 4 October 2020
Available online 9 October 2020

Keywords:
Numerical simulation
Compressible flow
Shock-capturing scheme
TENO scheme
Adaptive dissipation

ABSTRACT

High fidelity numerical simulation of compressible flow requires the numerical method being used to have both stable shock-capturing capability and high spectral resolution. Recently, a family of Targeted Essentially Non-Oscillatory (TENO) schemes is developed to fulfill such requirements. Although TENO has very low dissipation for smooth flow, it introduces a cutoff value C_T to maintain the non-oscillatory shock-capturing property. As C_T actually controls the dissipation property of TENO, the choice of C_T for better shock-capturing capability also means higher dissipation for small structures. To overcome this, in this paper, a new local adaptive method is proposed for the choice of C_T. By introducing a novel adaptive function based on the WENO smoothness indicators, C_T is dynamically adjusted from 1.0×10^{-10} for lower dissipation to 1.0×10^{-4} for stable capturing of shock according to the smoothness of the reconstruction stencil. The numerical results of the new method are compared with those of the original TENO method and an adaptive TENO method in Fu et al. (2019) [49]. It reveals that the new method is capable of suppressing numerical oscillations near discontinuities while further improving the resolution of TENO at a low extra computational cost.

1. Introduction

Compressible flow is ubiquitous in engineering and scientific researches. It is featured by multi-scale spatial/temporal structures like turbulence, discontinuities like shockwaves, and the interactions of such structures. Accurate and high fidelity numerical simulation of compressible flow requires numerical methods that are capable of simultaneously resolving all of these flow phenomena. However, different structures have different demands: low-dissipation for multi-scale structures and high-dissipation for discontinuities. Such contradictory requirements imply that a numerical scheme should be able to adjust its dissipation property in accordance with the flow structure being locally resolved.

The state-of-the-art study of numerical methods for compressible flow concerns the development of high-order shock-capturing schemes. Such methods suppress numerical oscillations in the vicinity of discontinuities by increasing dissipation when the local gradient is large enough while maintaining low dissipation in smooth regions.

By using intrinsic limiting procedures, classical high-order shock-capturing schemes, as exemplified by total variation diminishing (TVD) schemes [1], essentially non-oscillatory (ENO) schemes [2], and so on [3], can resolve discontinuities

* Corresponding author.
E-mail addresses: pengjun@imech.ac.cn (J. Peng), yqshen@imech.ac.cn (Y. Shen).

https://doi.org/10.1016/j.jcp.2020.109902
0021-9991/

without numerical oscillations; nevertheless, they suffer from excessive numerical dissipation in smooth regions. The family of weighted essentially non-oscillatory (WENO) finite difference schemes [4,5] achieves lower dissipation for smooth fields as well as non-oscillatory shock-capturing capability. Based on the smoothness of each sub-stencil, WENO schemes dynamically adjust local numerical dissipation in an elaborate weighting approach. Within the general framework of the WENO-JS scheme by Jiang & Shu [5], the WENO family is further extended and developed. Henrick et al. [6] found that the WENO-JS scheme, at critical points, does not satisfy the fifth-order convergence conditions, and the WENO-M scheme was proposed to circumvent such problem by mapping of the WENO-JS weights. Borges et al. [7] introduced a higher-order smoothness indicator for the non-linear weights and proposed the WENO-Z scheme which satisfies the sufficient criteria for fifth-order convergence at much lower computational cost than the WENO-M method. The accuracy of the WENO-Z scheme was further improved in [8–13]. Shen and Zha [14] showed that at transitional points, which connect smooth region and discontinuity, the accuracy of fifth-order WENO schemes is second-order and a series of multi-step weighting methods [15–18] were developed to improve the accuracy. Other high-order methods were also developed based on the ideal of WENO in [19–25]. Even though the order of accuracy for WENO schemes can be designed to be arbitrarily high [26–29], the spectral resolution of WENO schemes is still not satisfactory [30]. Specifically, their excessive numerical dissipation for small scale structures in compressible turbulent flows may overwhelm physical dissipation [31]. Compared to linear schemes of the same order, such high dissipation is related to the weighting mechanism and the smoothness indicators of the WENO scheme.

By using a switcher/shock-sensor to classify the flow field as smooth or discontinuous, hybrid schemes [32–35] apply low dissipation schemes such as compact schemes [36] in smooth regions and shock-capturing schemes such as the WENO scheme when discontinuities emerge. The high dissipation caused by the weighting mechanism of WENO for smooth regions is thus avoided. Varieties of methods have been proposed to develop switcher/shock-sensor method [37,38,3], such as the flow variable difference between neighboring points [32–34], the flow gradients [31,39], the multi-resolution coefficients [35,40], and the Boundary Value Diminishing (BVD) criterion [41,42]. Obviously, the performance of a hybrid scheme relies on the accuracy of its switcher/shock-sensor.

Beyond typical WENO and hybrid approaches, a novel way to control numerical dissipation was introduced in the family of targeted ENO (TENO) schemes [43–45]. By using a scale separation technique [46], TENO cuts off the least smooth sub-stencil and therefore avoids the high dissipation issue caused by the WENO weights. The idea of TENO can be extended to arbitrarily high order [47,48]. TENO achieves significant low dissipation for smooth fields; however, it still produces numerical oscillations for some strong discontinuities if the cutoff value C_T used is inappropriate. With constant C_T, better shock-capturing capability also leads to higher dissipation for small structures, a compromise between shock-capturing and small structure resolution is inevitable. Based on a non-linear shock detector, an adaptive version of C_T was developed in [45,49]. This adaptive TENO scheme (TENO-A) increases C_T near discontinuities for non-oscillatory shock-capturing and uses smaller C_T in smooth regions for higher resolution. Compared to TENO, TENO-A achieves higher resolution and maintains shock-capturing capability at the price of higher computational cost. Although TENO-A performs very well for most problems, the shock detector requires a compromise between low dissipation and good ENO property if the problem considered becomes more complicated, as discussed in [50].

In this paper, we propose a new adaptive method to improve the performance of TENO as well as TENO-A. Based on the shock-sensor developed in [51], a novel adaptive function for C_T is introduced. The new method maintains the low dissipation property of TENO for smooth fields and maintains its shock-capturing capability at a low price. This paper is organized as follows. In Sec. 2, the TENO scheme is briefly reviewed. The new method is proposed and analyzed in Sec. 3. Numerical validations are presented in Sec. 4. Concluding remarks are given in 5.

2. The fifth-order targeted ENO scheme of Fu et al. [43,45,49]

To describe the TENO scheme, we consider the one-dimensional hyperbolic conservation law expressed as:

$$\frac{\partial u}{\partial t}+\frac{\partial f}{\partial x}=0 \tag{1}$$

where $u(x,t)$ is the conserved variable and $f(u)$ is the flux function. To solve (1) numerically, we transform it into semi-discretized form on uniformly discretized space:

$$\frac{du_i}{dt}=-\frac{\hat{f}_{i+\frac{1}{2}}-\hat{f}_{i-\frac{1}{2}}}{\Delta x} \tag{2}$$

in which $u_i=u(x_i)$, $\hat{f}_{i+\frac{1}{2}}=\hat{f}^{+}_{i+\frac{1}{2}}+\hat{f}^{-}_{i+\frac{1}{2}}$ is the numerical flux at cell interface $x_{i+\frac{1}{2}}=x_i+\Delta x/2$ and $\Delta x=x_{i+1}-x_i$. The splitted numerical fluxes $\hat{f}^{\pm}_{i+\frac{1}{2}}$ at cell interface are to be reconstructed. For simplicity, $\pm$ in the superscript are dropped in the following parts of this paper.

The numerical flux $\hat{f}_{i+\frac{1}{2}}$ can be obtained by high order schemes. The fifth -rder upstream-biased scheme is written as:

$$\hat{f}_{i+\frac{1}{2}}=\frac{2}{60}f_{i-2}-\frac{13}{60}f_{i-1}+\frac{47}{60}f_i+\frac{27}{60}f_{i+1}-\frac{3}{60}f_{i+2}, \tag{3}$$

where $f_i = f(u_i)$ is the point value of the flux. Eq. (3) is a convex combination of three third order schemes on three sub-stencils $S_0 = (x_{i-2}, x_{i-1}, x_i)$, $S_1 = (x_{i-1}, x_i, x_{i+1})$, and $S_2 = (x_i, x_{i+1}, x_{i+2})$:

$$\hat{f}_{0,i+1/2} = \frac{1}{3}f_{i-2} - \frac{7}{6}f_{i-1} + \frac{11}{6}f_i, \tag{4}$$

$$\hat{f}_{1,i+1/2} = -\frac{1}{6}f_{i-1} + \frac{5}{6}f_i + \frac{1}{3}f_{i+1}, \tag{5}$$

$$\hat{f}_{2,i+1/2} = \frac{1}{3}f_i + \frac{5}{6}f_{i+1} - \frac{1}{6}f_{i+2} \tag{6}$$

with linear weights

$$c_0 = 0.1, \quad c_1 = 0.6, \quad c_2 = 0.3$$

respectively. For higher spectral resolution, the optimized weights can be applied as in [49]:

$$c_0 = 0.1235341937, \quad c_1 = 0.5065006634, \quad c_2 = 0.3699651429.$$

By substituting the linear weights with the non-linear TENO weights, we have the fifth-rder TENO scheme, which has the same form as the WENO scheme:

$$\text{TENO5}: \quad \hat{f}_{i+1/2} = \omega_0 \hat{f}_{0,i+1/2} + \omega_1 \hat{f}_{1,i+1/2} + \omega_2 \hat{f}_{2,i+1/2}. \tag{7}$$

To compute the non-linear weights ω_k, the smoothness of each sub-stencil is firstly measured by:

$$\gamma_k = \left(C + \frac{\tau_K}{\beta_k + \epsilon}\right)^q, k = 0, 1, 2 \tag{8}$$

in which τ_K is the global smoothness indicator, β_k is the WENO smoothness indicator [5] of each sub-stencil given by:

$$\beta_0 = \frac{13}{12}(f_{i-2} - 2f_{i-1} + f_i)^2 + \frac{1}{4}(f_{i-2} - 4f_{i-1} + 3f_i)^2, \tag{9}$$

$$\beta_1 = \frac{13}{12}(f_{i-1} - 2f_i + f_{i+1})^2 + \frac{1}{4}(f_{i-1} - f_{i+1})^2, \tag{10}$$

$$\beta_2 = \frac{13}{12}(f_i - 2f_{i+1} + f_{i+2})^2 + \frac{1}{4}(3f_i - 4f_{i+1} + f_{i+2})^2. \tag{11}$$

Noted that the choice for τ_K is flexible for TENO [43]. The global smoothness indicator of WENO-Z, i.e.:

$$\tau_K = \tau_5 = |\beta_2 - \beta_0| \tag{12}$$

is used in this paper. C and q are parameters to incorporate a scale-separation mechanism [46] with typical values $C = 1$ and $q = 6$. ϵ is a small value to avoid division by zero as in the WENO scheme. ϵ is set to 1×10^{-40} in this paper.

Then, a ENO-like stencil selection method is applied. The smoothness measure Eq. (8) is normalized:

$$\chi_k = \frac{\gamma_k}{\sum_{k=0}^{2}\gamma_k}, \quad k = 0, 1, 2 \tag{13}$$

and passed to a cutoff function:

$$\delta_k = \begin{cases} 0 & \chi_k < C_T, \\ 1 & \text{otherwise.} \end{cases} \tag{14}$$

Typically C_T is set to be 1×10^{-5} [43].

Finally, the non-linear TENO weights are computed as:

$$\omega_k = \frac{\delta_k c_k}{\sum_{k=0}^{2}\delta_k c_k}, \quad k = 0, 1, 2. \tag{15}$$

The dissipation property of TENO is related to the choice of the cutoff value C_T [43,44]. Smaller C_T brings lower dissipation but may also lead to numerical oscillations. An adaptive C_T is proposed in [45,49]:

$$\begin{cases} C_T & = 10^{-\lfloor \beta \rfloor}, \\ \beta & = \alpha_1 - \alpha_2(1 - g(m)), \\ g(m) & = (1-m)^4(1+4m), \end{cases} \tag{16}$$

where

$$\begin{cases} m & = 1 - min(1, \frac{\eta_{i+1/2}}{C_r}) \\ \eta_{i+1/2} & = min(\eta_{i-1}, \eta_i, \eta_{i+1}) \end{cases} \tag{17}$$

in which

$$\eta_i = \frac{2|\Delta f_{i+1/2}\Delta f_{i-1/2}| + \epsilon}{(\Delta f_{i+1/2})^2 + (\Delta f_{i+1/2})^2 + \epsilon}, \quad \Delta f_{i+1/2} = f_{i+1} - f_i, \quad \epsilon = \frac{0.9C_r}{1 - 0.9C_r}\xi^2, \tag{18}$$

and $\lfloor\cdot\rfloor$ denotes the floor function. The values of the parameters are $\alpha_1 = 10.0$, $\alpha_2 = 5.0$, $C_r = 0.24$, and $\xi = 10^{-3}$ [49]. The setup (16) gives C_T a dynamically adjustable interval according to the smoothness of the flow field ranging from 10^{-5} for shock-capturing to 10^{-10} for low dissipation. The TENO scheme with adaptive C_T Eq. (16) is referred to as TENO5-A.

3. The new method

The adaptive method (16) for C_T brings extra computational cost. Besides, more free parameters (C_r, α_1, α_2, and ξ) are introduced. As will be shown latter, the adaptive method Eq. (16) is insufficient to suppress numerical oscillations for some strong discontinuities.

To design a more efficient adaptive C_T, we propose the following principles:

- The adaptive method only uses information that has already been provided by the WENO part, e.g., β_k, τ_K.
- The upper and lower bounds of C_T are given by magnitudes instead of values.
- The fewer free parameters, the better.

Following these principles, we propose a new adaptive C_T:

$$\begin{cases} C_T & = 10^{-m}, \\ m & = B_l + \lfloor\theta(B_u - B_l)\rfloor, \end{cases} \tag{19}$$

where

$$\theta = \frac{1}{1 + \left(\max_k \tilde{\chi}_k / H\right)}, \quad \tilde{\chi}_k = \frac{\tau_K}{\beta_k + \epsilon}, \quad k = 0, 1, 2. \tag{20}$$

θ is the Runge function that it has been used as shock-sensor [16] and switcher [52] to design adaptive methods. H is the intensity threshold for discontinuities. For example, by taking $H = 10$, it means that if the maximum of $\tilde{\chi}_k$ is over 10 then the whole stencil is considered to be discontinuous. Parameters B_l and B_u are the lower and upper magnitudes of C_T. Typical values of B_l and B_u are:

$$B_l = 4, \quad B_u = 10.$$

According the smoothness of the stencil, θ varies from 0 for discontinuity to 1 for smooth field. The value of C_T therefore varies from 10^{-B_l} to 10^{-B_u}. Noted that C_T equals 10^{-B_u} only when θ is exactly 1.0, i.e. $\max_k \tilde{\chi}_k / H = 0.0$.

Considering that the computational cost for computing 10^{-m} on computer is very high. We introduce a constant array, the Ladder array, to store pre-calculated C_Ts of different magnitudes:

$$\text{Ladder}: \quad Lad(B_l : B_u) = (10^{-B_l}, ..., 10^{-B_u}). \tag{21}$$

C_T is then determined by:

$$C_T = Lad(m). \tag{22}$$

In the following part of the paper, we refer to the new method as TENO5-LAD (Local Adaptive Dissipation)

Spectral properties of TENO5-LAD and the linear fifth-order upwind scheme, the WENO-Z scheme, and TENO schemes with different C_Ts are illustrated in Fig. 1. The new scheme maintains the good spectral property of the TENO scheme. It is worth noting that although TENO5-A shows lower dissipation and dispersion error at high wavenumbers, it is unable to suppress numerical oscillations, as will be shown in Sec. 4.

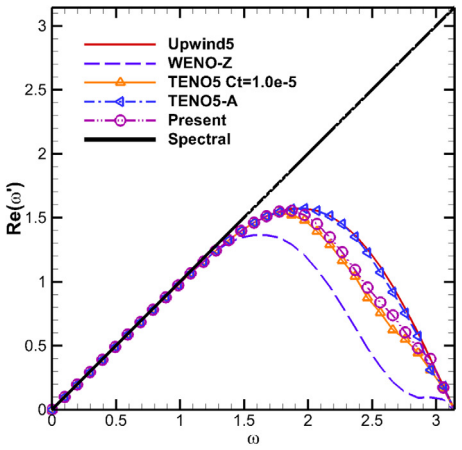

(a) Dispersion

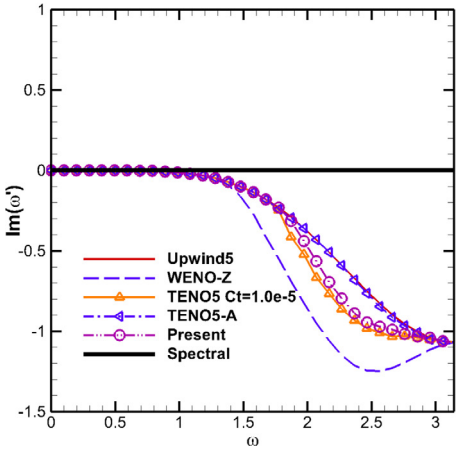

(b) Dissipation

Fig. 1. Dispersion and dissipation properties of different schemes.

4. Numerical validation

To assess the new method, we perform several numerical tests, including 1D scalar, 1D Euler, and 2D Euler problems. Numerical results are compared with TENO schemes with different C_T setups as well as WENO-Z. Unless specified, C_T for TENO5 is set to be 10^{-5}, the parameters of the TENO5-A scheme is taken as:

$$a_1 = 10.0, \quad a_2 = 5.0, \quad C_r = 0.24, \quad \xi = 10^{-3},$$

and the parameters of the presented method is set to be:

$$H = 10.0, \quad B_l = 4.0, \quad B_u = 10.0.$$

As the main theme of this paper is to develop an adaptation method, therefore, if not specified, the canonical sub-stencil weights (the standard WENO values) are used for the tested TENO schemes for better comparison purposes. Considering that the parameters of TENO5-A are designed for the optimized weights, for completeness, results computed with the optimized weights are also provided for the tested TENO schemes for some cases.

For all of the numerical tests in this section, the third order TVD Runge-Kutta method [53] is used for time advancing:

$$u^{(1)} = u^n + \Delta t L(u^n) \tag{23}$$

$$u^{(2)} = \frac{3}{4}u^n + +\frac{1}{4}u^{(1)} + \frac{1}{4}\Delta t L(u^{(1)}) \tag{24}$$

$$u^{n+1} = \frac{1}{3}u^n + \frac{2}{3}u^{(2)} + \frac{2}{3}\Delta t L(u^{(2)}). \tag{25}$$

Table 1
L_2 errors and convergence orders for different schemes for the linear advection equation with initial condition (30) at t=2.

N	Upwind5		TENO5		TENO5-A		Present	
	L_2	order	L_2	order	L_2	order	L_2	order
20	2.7611E-003	-	2.7611E-003	-	2.7611E-003	-	2.7611E-006	-
40	9.5732E-005	4.85	9.5732E-004	4.85	9.5732E-004	4.85	9.5732E-006	4.85
80	3.0514E-006	4.97	3.0514E-006	4.97	3.0514E-006	4.97	3.0514E-006	4.97
160	9.6010E-008	4.99	9.6010E-007	4.99	9.6010E-007	4.99	9.6010E-006	4.99
320	3.0061E-009	5.00	3.0061E-009	5.00	3.0061E-009	5.00	3.0061E-006	5.00

Unless specified, the time step Δt is given by:

$$\Delta t = \sigma \frac{\Delta x}{\max\limits_i(|u_i| + \alpha_i)} \tag{26}$$

for one dimensional cases and

$$\Delta t = \sigma \frac{\Delta t_x \Delta t_y}{\Delta t_x + \Delta t_y},\ \Delta t_x = \frac{\Delta x}{\max\limits_{i,j}(|u_{i,j}| + \alpha_{i,j})},\ \Delta t_y = \frac{\Delta y}{\max\limits_{i,j}(|v_{i,j}| + \alpha_{i,j})} \tag{27}$$

for two dimensional cases, where σ is the Courant-Friedrichs-Lewy number. If not specified, the CFL number is set as 0.2 for all cases. It should be noted that a small CFL number is chosen in this paper to reduce the influence of time advancing method to evaluate the new scheme's performance better. The effect of the CFL number on TENO schemes can be found in [43,49].

For the convective terms, the global Lax-Friedrichs splitting method [54] is used, and the reconstruction of the numerical flux is performed in the characteristic space [55].

4.1. Linear advection equation

Let us consider the linear wave advection problem. The linear advection equation is given by:

$$\begin{cases} u_t + u_x = 0 & -1 \leqslant x \leqslant 1, \\ u(x,0) = u_0(x) & \text{periodic boundary.} \end{cases} \tag{28}$$

The exact solution of Eq. (28) at time t with the initial condition $u_0(x)$ is given by

$$u(x,t) = u_0(x-t). \tag{29}$$

Two cases are studied in this section.

The first case is to evaluate the convergence order of the present scheme for a smooth solution. The initial condition is given by:

$$u_0(x) = sin(\pi x - \frac{sin\pi x}{\pi}). \tag{30}$$

This initial condition has two critical points where $f' = 0$ and $f''' \neq 0$ [6]. The time step Δt is set to $\Delta x^{5/3}$.

The L_2 norm of the error is obtained by comparison with the exact solution at $t = 2$ according to:

$$L_2 = \sqrt{\frac{1}{N}\sum_{i=1}^{N}\left(u_i - u_{exact,i}\right)^2}$$

Table 1 shows the L_2 norms as well as convergence orders for different schemes. The differences of L_2 errors between different schemes are trivial.

The initial condition of the second case is:

$$u_0(x) = \begin{cases} \frac{1}{6}(G(x,\beta,z-\delta) + G(x,\beta,z+\delta) + 4G(x,\beta,z)), & -0.8 \leqslant x < -0.6 \\ 1, & -0.4 \leqslant x < -0.2 \\ 1 - |10(x-0.1)|, & 0 \leqslant x < 0.2 \\ \frac{1}{6}(F(x,\alpha,a-\delta) + F(x,\alpha,a+\delta) + 4F(x,\alpha,a)), & 0.4 \leqslant x < 0.6 \\ 0, & \text{otherwise} \end{cases} \tag{31}$$

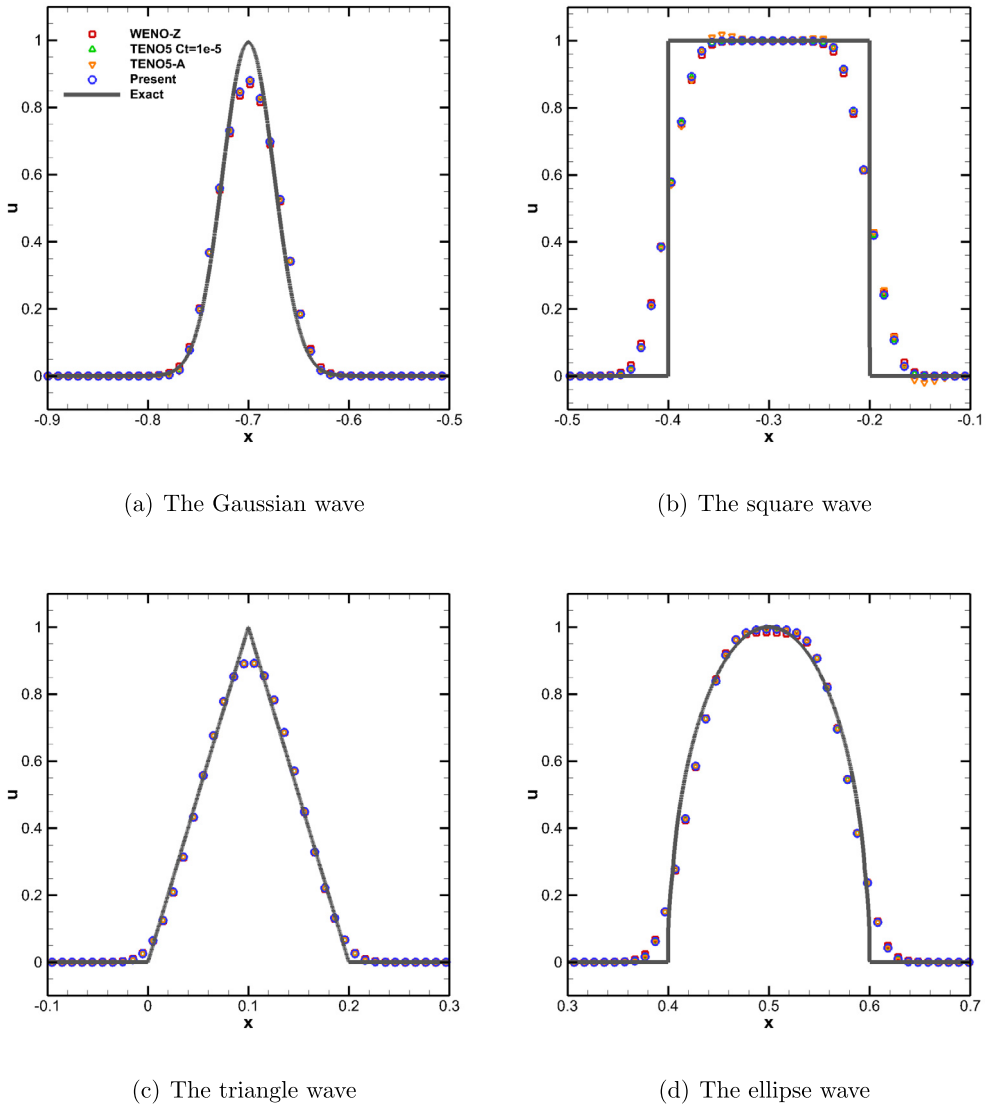

(a) The Gaussian wave (b) The square wave

(c) The triangle wave (d) The ellipse wave

Fig. 2. Results of the linear advection equation with the initial condition (31) at t=6, N=200.

where

$$G(x,\beta,z)=e^{-\beta(x-z)^2},\ F(x,\alpha,a)=\sqrt{max(1-\alpha^2(x-a)^2,0)},$$
$$a=0.5,z=-0.7,\delta=0.005,\alpha=10,\beta=log2/36\delta^2.$$

The solution of Eq. (31) contains a smooth but narrow combination of Gaussians, a square wave, a sharp triangle wave, and a half ellipse [5]. As this test case is a combination of both smooth and non-smooth functions, it has been widely used to test the discontinuity capturing capability of a scheme.

Numerical results of different schemes are given in Fig. 2. It can be observed that TENO5-A produces oscillations for the square wave while the others not. The presented method well preserves the ENO property for the discontinuities and maintains low dissipation for the smooth waves.

Consider an extreme condition. Solution of the initial condition (31) scaled by a factor of 10^{-3} are given in Fig. 3. It can be observed that TENO5-A generates obvious oscillations while TENO5 and TENO5-LAD obtain almost identical results with respect to the non-scaled result. It indicates that the adaptation method of TENO5-A with the chosen parameters is not scalar invariant for such circumstances.

It should be pointed out that, for this kind of extreme cases, the numerical oscillations of TENO5-A maybe caused by the non-smoothness measurement of Eq. (18) which is not functioning well with the chosen ϵ, and the user may use a proper small value of ϵ according to their problem or machine to overcome this deficiency. However, it is difficult for a

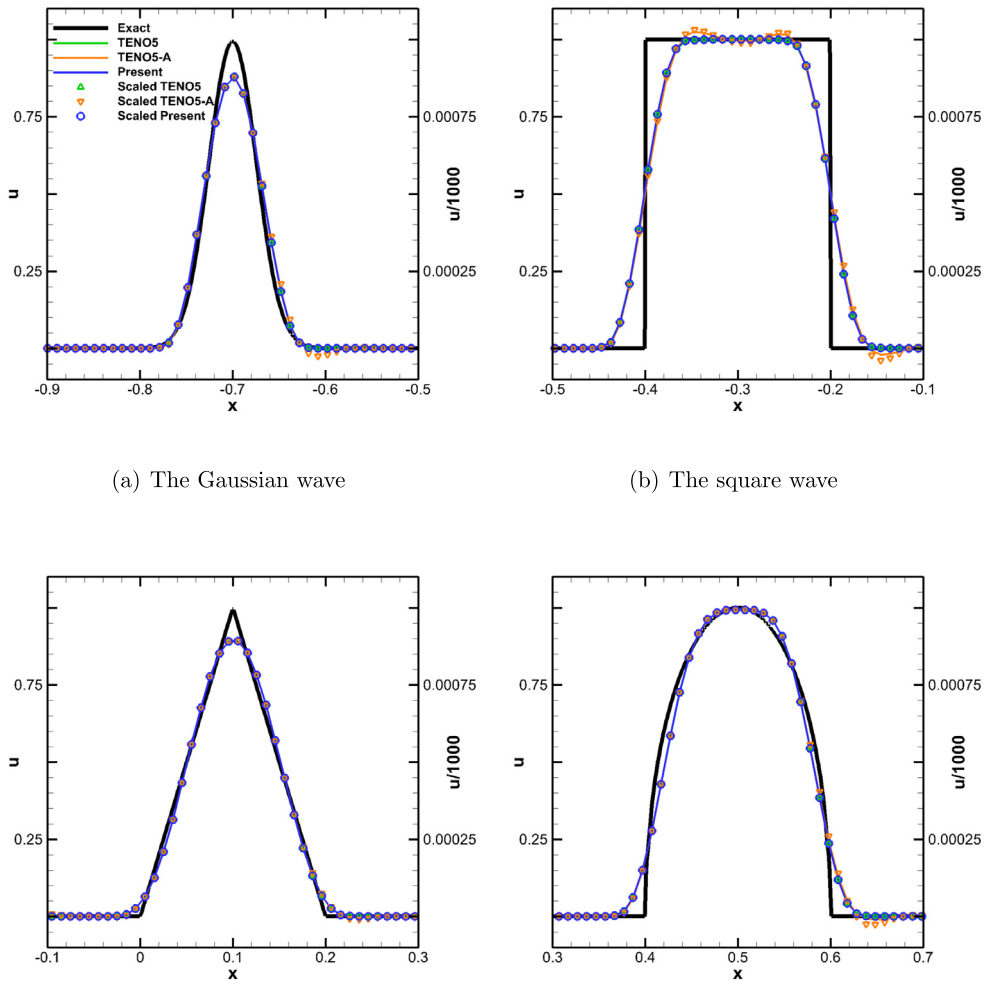

(a) The Gaussian wave

(b) The square wave

(c) The triangle wave

(d) The ellipse wave

Fig. 3. Results of the linear advection equation with the initial condition (31) scaled by a factor of 10^{-3} at t=6, N=200. (For interpretation of the colors in the figure(s), the reader is referred to the web version of this article.)

complex problem to choose a proper value to maintain both high accuracy and oscillation free [50]. Developing robust and problem-independent methods is still an open issue.

4.2. One dimensional Euler equations

The one dimensional Euler equations are given by

$$U_t + F(U)_x = 0 \tag{32}$$

where $U = (\rho, \rho u, e)^T$ and $F(U) = (\rho u, \rho u^2 + p, u(e + p))^T$. Here ρ is the density, u is the velocity, e is the total energy, p is the pressure, and for ideal gas $e = \frac{p}{\gamma - 1} + \frac{1}{2}\rho u^2$, $\gamma = 1.4$ is the ratio of specific heat.

Six typical examples containing strong discontinuities are considered here. The first example is the Sod problem [5]. The initial conditions are:

$$(\rho, u, p) = \begin{cases} (1, 0, 1) & x \leqslant 0 \\ (0.125, 0, 0.1) & x > 0 \end{cases} \tag{33}$$

with zero gradient boundary conditions applied at $x = \pm 0.5$.

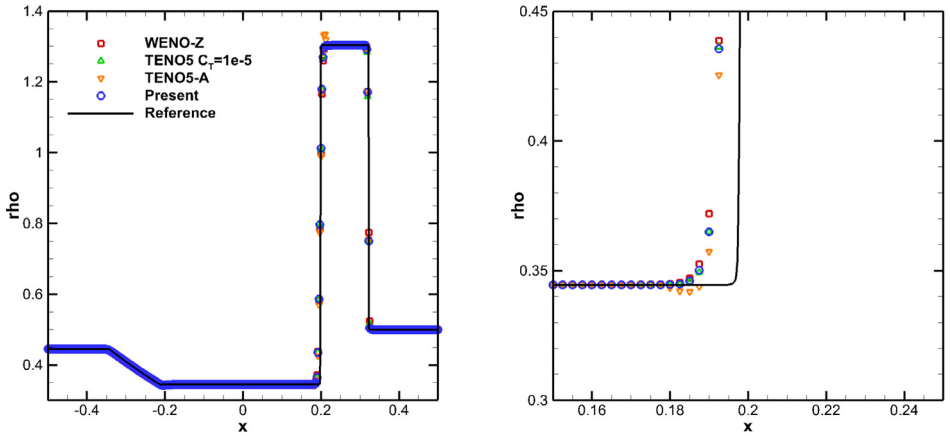

(a) Density distribustion (b) Zoom-in view

Fig. 4. Results of different schemes for the Lax problem, t=0.13, N=400.

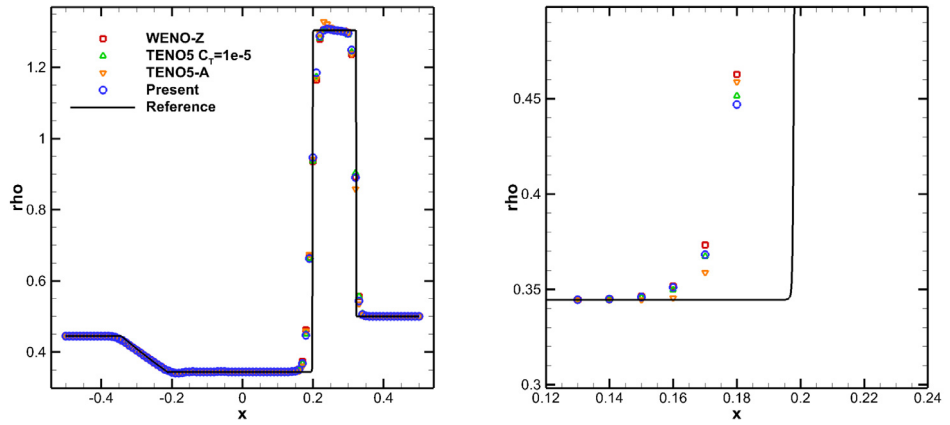

(a) Density distribustion (b) Zoom-in view

Fig. 5. Results of different schemes for the Lax problem with CFL=0.2, t=0.13, N=100.

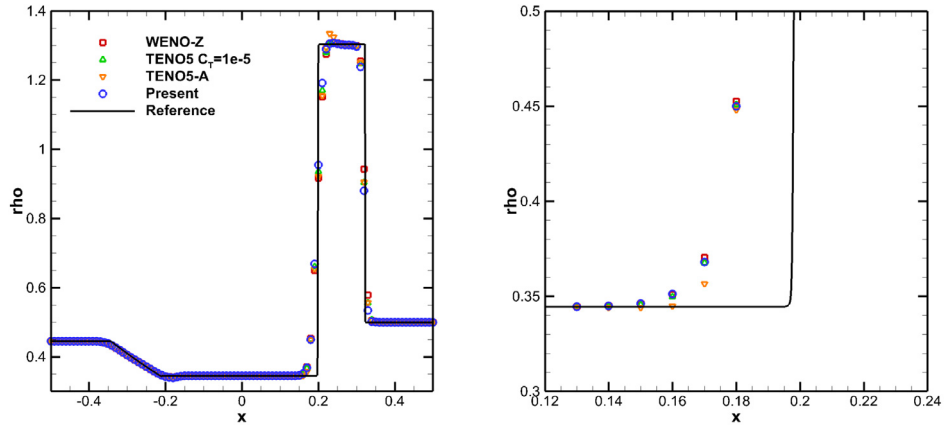

(a) Density distribustion (b) Zoom-in view

Fig. 6. Results of different schemes for the Lax problem with CFL=0.4, t=0.13, N=100.

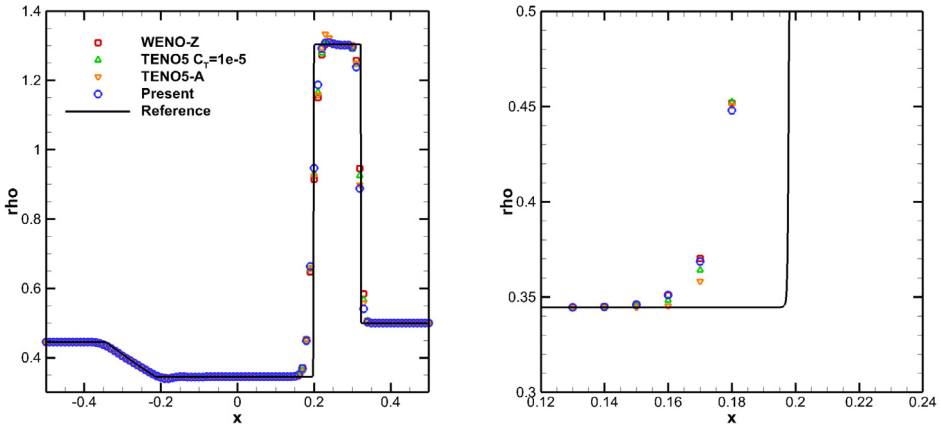

(a) Density distribustion (b) Zoom-in view

Fig. 7. Results of different schemes for the Lax problem with CFL=0.6, t=0.13, N=100.

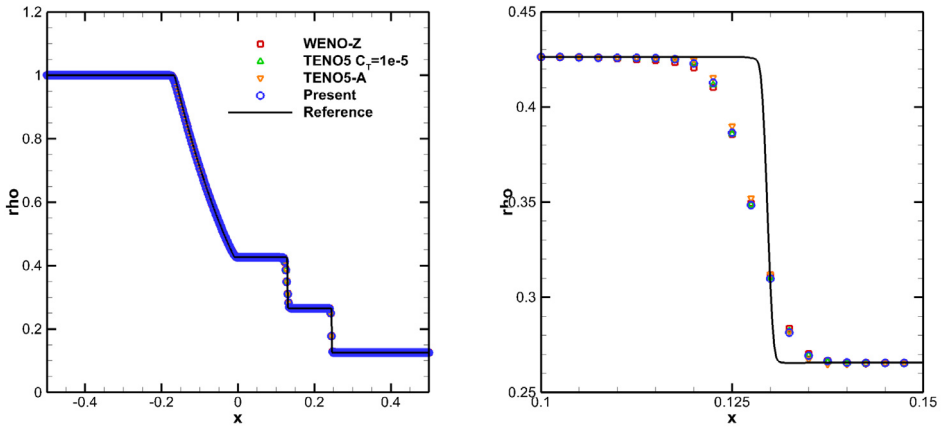

(a) Density distribustion (b) Zoom-in view

Fig. 8. Results of different schemes for the Sod problem, t=0.14, N=400.

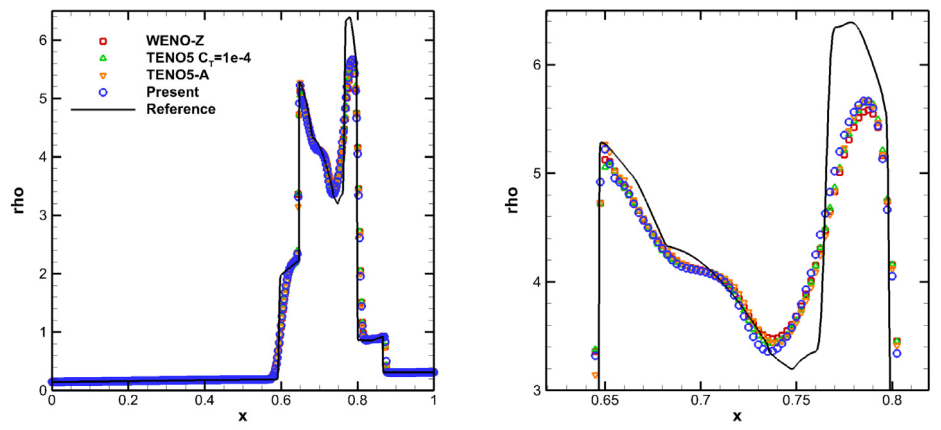

(a) Density distribustion (b) Zoom-in view

Fig. 9. Results of different schemes for the two interacting blast waves problem, t=0.038, N=400.

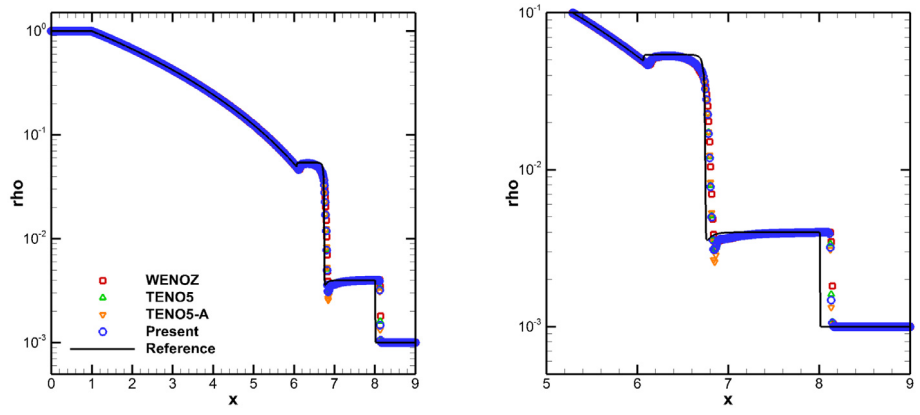

(a) Density distribustion (b) Zoom-in view

Fig. 10. Results of different schemes for the Le Blanc problem, t=6.0, N=800.

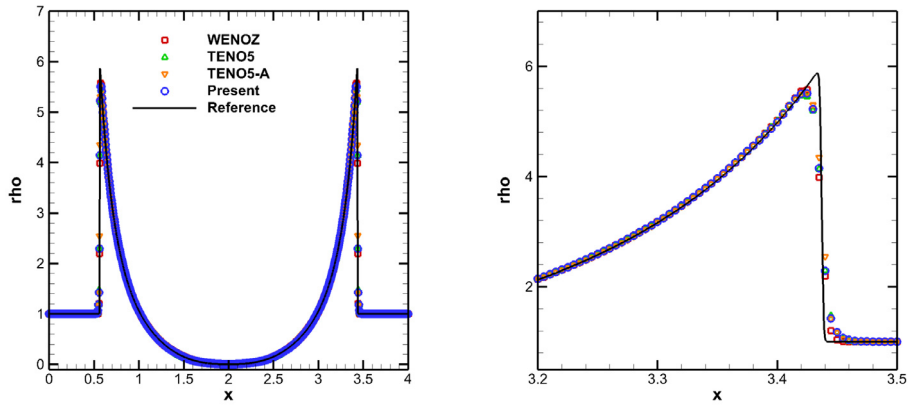

(a) Density distribustion (b) Zoom-in view

Fig. 11. Results of different schemes for the Sedov problem, t=0.001, N=800.

The second problem is the Lax problem [5], the initial conditions are given by:

$$(\rho, u, p) = \begin{cases} (0.445, 0.698, 3.528) & x \leqslant 0 \\ (0.5, 0, 0.571) & x > 0 \end{cases} \tag{34}$$

with zero gradient boundary conditions at $x = \pm 0.5$.

The third problem is the two interacting blast waves case [56]. The initial conditions are given by:

$$(\rho, u, p) = \begin{cases} (1, 0, 1000) & 0 \leqslant x < 0.1 \\ (1, 0, 0.01) & 0 \leqslant x < 0.9 \\ (1, 0, 100) & 0.9 \leqslant x \leqslant 1. \end{cases} \tag{35}$$

Zero gradient boundary conditions are set at boundaries.

The fourth problem is the Le Blanc problem [57]. The initial conditions are given by:

$$(\rho, u, p) = \begin{cases} (1, 0, \frac{2}{3} \times 10^{-1}) & 0 \leqslant x \leqslant 3 \\ (1, 0, \frac{2}{3} \times 10^{-10}) & 3 < x \leqslant 9. \end{cases} \tag{36}$$

Zero gradient boundary conditions are set at boundaries.

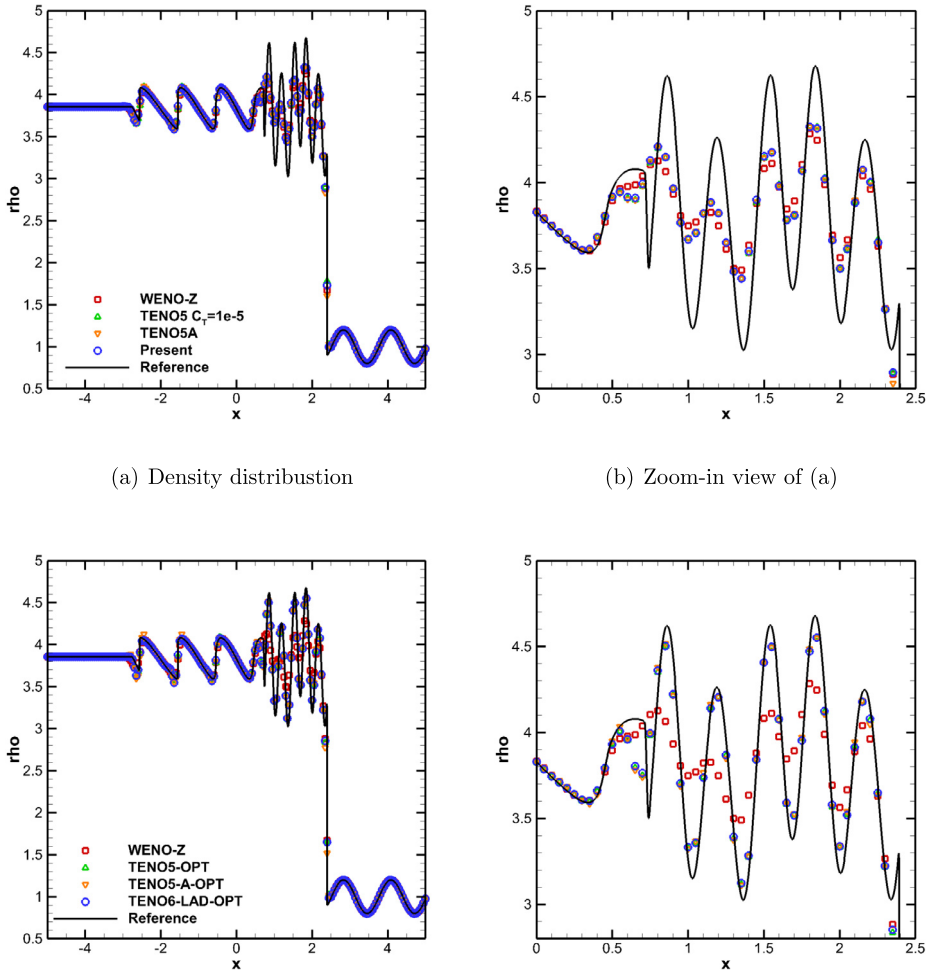

(a) Density distribustion

(b) Zoom-in view of (a)

(c) Density distribustion computed with optimized weights

(d) Zoom-in view of (c)

Fig. 12. Results of different schemes for the Shu-Osher problem, N=200, t=1.8.

The fifth problem is the Sedov problem [57]. The initial conditions are given by:

$$(\rho, u, p) = \begin{cases} (1, 0, 1.28 \times 10^6/\Delta x) & 2 - 0.5\Delta x \leqslant x \leqslant 2 + 0.5\Delta x \\ (1, 0, 4.0 \times 10^{-13}) & \text{otherwise,} \end{cases} \tag{37}$$

where Δx is the grid size. Zero gradient boundary conditions are set at $x = 0.0$ and $x = 4.0$.

The last problem is the Shu-Osher problem [5]. It describes the interaction of a Mach 3 shock with a density wave. The initial conditions are given by:

$$(\rho, u, p) = \begin{cases} (\frac{27}{7}, \frac{4\sqrt{35}}{9}, \frac{31}{3}) & x < -4 \\ (1 + \frac{1}{5}sin5x, 0, 1) & x \geqslant -4 \end{cases} \tag{38}$$

Zero gradient boundary conditions are applied at $x = \pm 5$.

Fig. 8 to Fig. 12 illustrate the results of the above cases. Reference results are obtained by the WENO-Z scheme with 2000 points.

For the sod problem, as shown in Fig. 8, each scheme resolves the discontinuities well. When the discontinuity becomes stronger for the Lax problem, as being shown in Fig. 4, the TENO5-A method produces oscillations near the contact wave. The presented method maintains the ENO property. Results computed with different CFL numbers on a $N = 100$ grid are also given in Figs. 5 to 7.

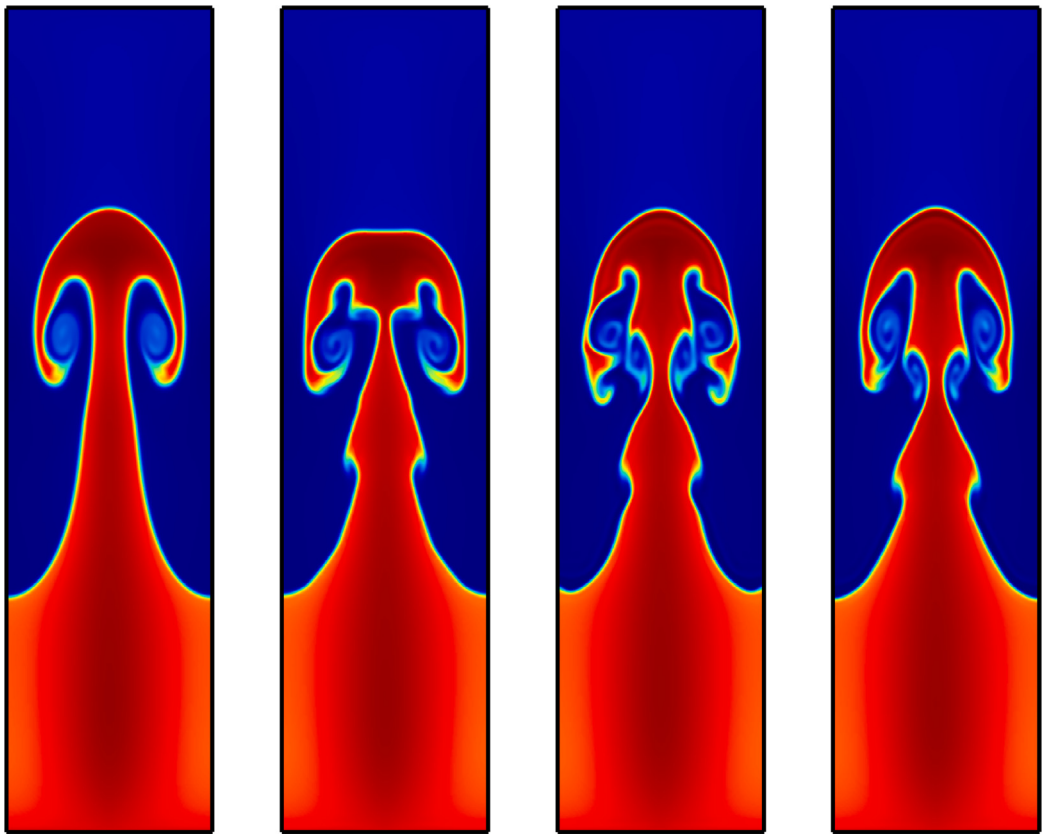

Fig. 13. Density contours of different schemes for the Rayleigh–Taylor instability problem at t=1.95 (blue = 0.85 to red = 2.25), $[N_x \times N_y] = [128 \times 512]$. (For interpretation of the colors in the figure(s), the reader is referred to the web version of this article.)

The two interacting blast waves problem is a more severe case with very strong discontinuities for high order schemes. C_T is adjusted to 10^{-4} for TENO5 to obtain a stable result. The upper bound of C_T of TENO5-A is also adjusted accordingly. From Fig. 9(b), it can be seen that the presented method obtains better-resolved structures than the others.

The Le Blanc problem and the Sedov problem involve even stronger pressure jumps and require stronger stability of a scheme. To calculate this kind of problem without the help of the positivity-preserving technique, C_T is adjusted to be 1.0^{-3} for the Le Blanc problem and 1.0^{-2} for the Sedov problem for TENO5. The upper bounds of C_T of TENO5-A and TENO5-LAD are also adjusted accordingly. C_r for TENO5-A is set to be 0.7 for the Le Blanc problem and 1.0 for the Sedov problem. The parameter H used by TENO5-LAD is 1.5 for both cases. Results in Fig. 10 and Fig. 11 show that the TENO schemes can handle such tough problems. TENO5-LAD obtains similar results near discontinuities as TENO5, indicating the effectiveness of the new adaptive function.

The results of the Shu-Osher problem are shown in Fig. 12. The TENO methods give better resolved short waves than the WENO-Z method. When computed with the optimized weights (see Fig. 12(d)), the TENO schemes obtain much better resolved short waves than WENOZ. The TENO schemes show similar results for the short waves; however, TENO5-A shows some overshoots near the shock waves (see Fig. 12(c)). The presented method better preserves the ENO property.

4.3. Two dimensional Euler equations

4.3.1. Rayleigh–Taylor instability

The two-dimensional Rayleigh-Taylor instability problem is often used to assess the dissipation property of a high-order scheme. It describes the interface instability between fluids with different densities when acceleration is directed from the heavy fluid to the light one. The acceleration effect is introduced by adding ρ and ρv to the y-momentum and the energy equations, respectively. The initial conditions are:

$$(\rho, u, v, p) = \begin{cases} (2, 0, -0.025\alpha cos(8\pi x), 2y + 1), & 0 \le y < 1/2, \\ (1, 0, -0.025\alpha cos(8\pi x), y + 3/2), & 1/2 \le y < 1, \end{cases} \tag{39}$$

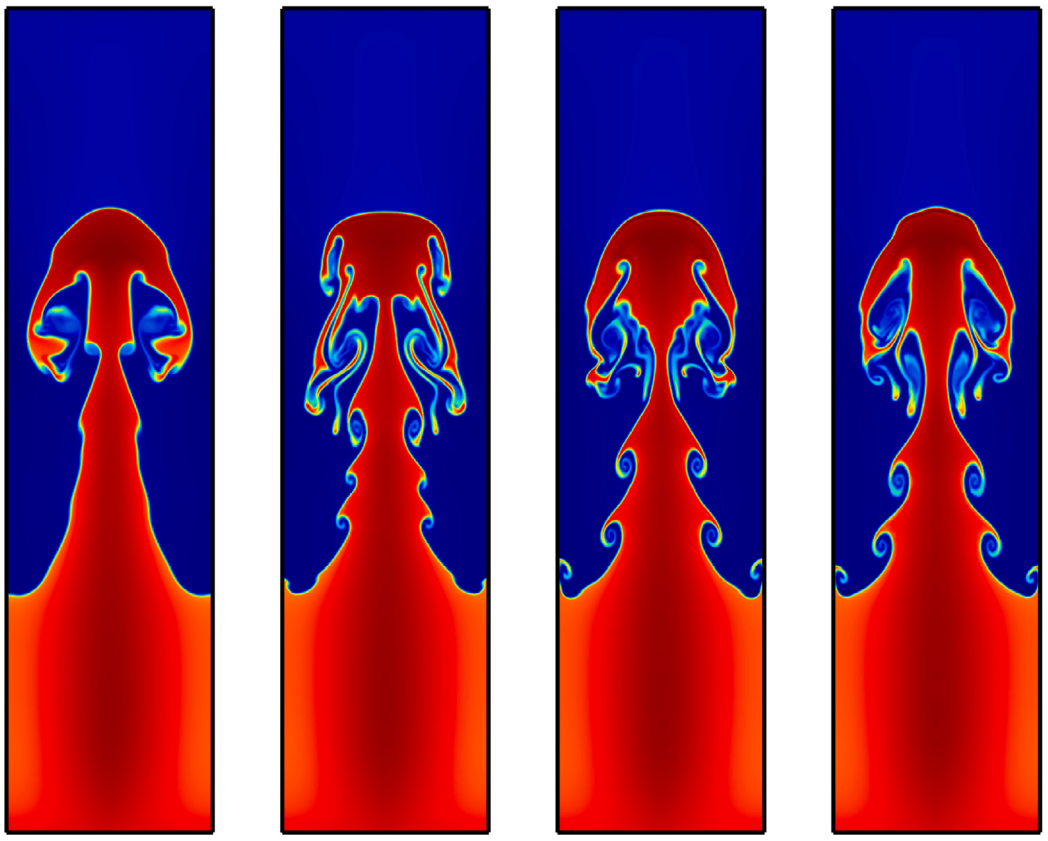

(a) WENO-Z (b) TENO5 (c) TENO5-A (d) Present

Fig. 14. Density contours of different schemes for the Rayleigh–Taylor instability problem at t=1.95 (blue = 0.85 to red = 2.25), $[N_x \times N_y] = [256 \times 1024]$. (For interpretation of the colors in the figure(s), the reader is referred to the web version of this article.)

where $\alpha = \sqrt{\gamma p/\rho}$ is the speed of sound with $\gamma = 5/3$. The computational domain is $[0, 0.25] \times [0, 1]$. The left and right boundaries are set with reflective boundary conditions, and the top and bottom boundaries are set as $(\rho, u, v, p) = (1, 0, 0, 2.5)$ and $(\rho, u, v, p) = (2, 0, 0, 1)$ respectively. The solution is integrated to $t = 1.95$.

Solutions on two sets of meshes are illustrated in Fig. 13 and Fig. 14. The TENO schemes resolve richer structures than the WENO-Z scheme. As the C_T ranges for TENO5-A and TENO5-LAD are the same, their results are similar that they both obtain richer structures compared to TENO5.

4.3.2. Riemann problems

Two 2D Riemann problems are considered in this section.

The first case corresponds to configuration 3 in [58] with the initial conditions

$$(\rho, u, v, p) = \begin{cases} (0.138,\ 1.206,\ 1.206,\ 0.029) & x \le 0.5,\ y \le 0.5, \\ (0.5323,\ 1.206,\ 0.0,\ 0.3) & x \le 0.5,\ y > 0.5, \\ (0.5323,\ 0.0,\ 1.206,\ 0.3) & x > 0.5,\ y \le 0.5, \\ (1.5,\ 0.0,\ 0.0,\ 1.5) & x > 0.5,\ y > 0.5. \end{cases} \tag{40}$$

Solutions are integrated to $t = 0.3$. A uniform grid of (1024×1024) is used.

Density contours are shown in Fig. 15. It can be seen that the TENO schemes present much richer K-H instability structures than the WENO-Z scheme. TENO5 and TENO5-LAD resolve more structures on the contact lines. As the parameters for TENO5-A are designed for optimized sub-stencil weights, the results of TENO schemes with optimized weights are shown in Fig. 16. It can be seen that with the optimized weights, TENO5-A better resolves the structures. The presented method gives a similar resolution of the structures as TENO5-A and also better maintains the ENO property.

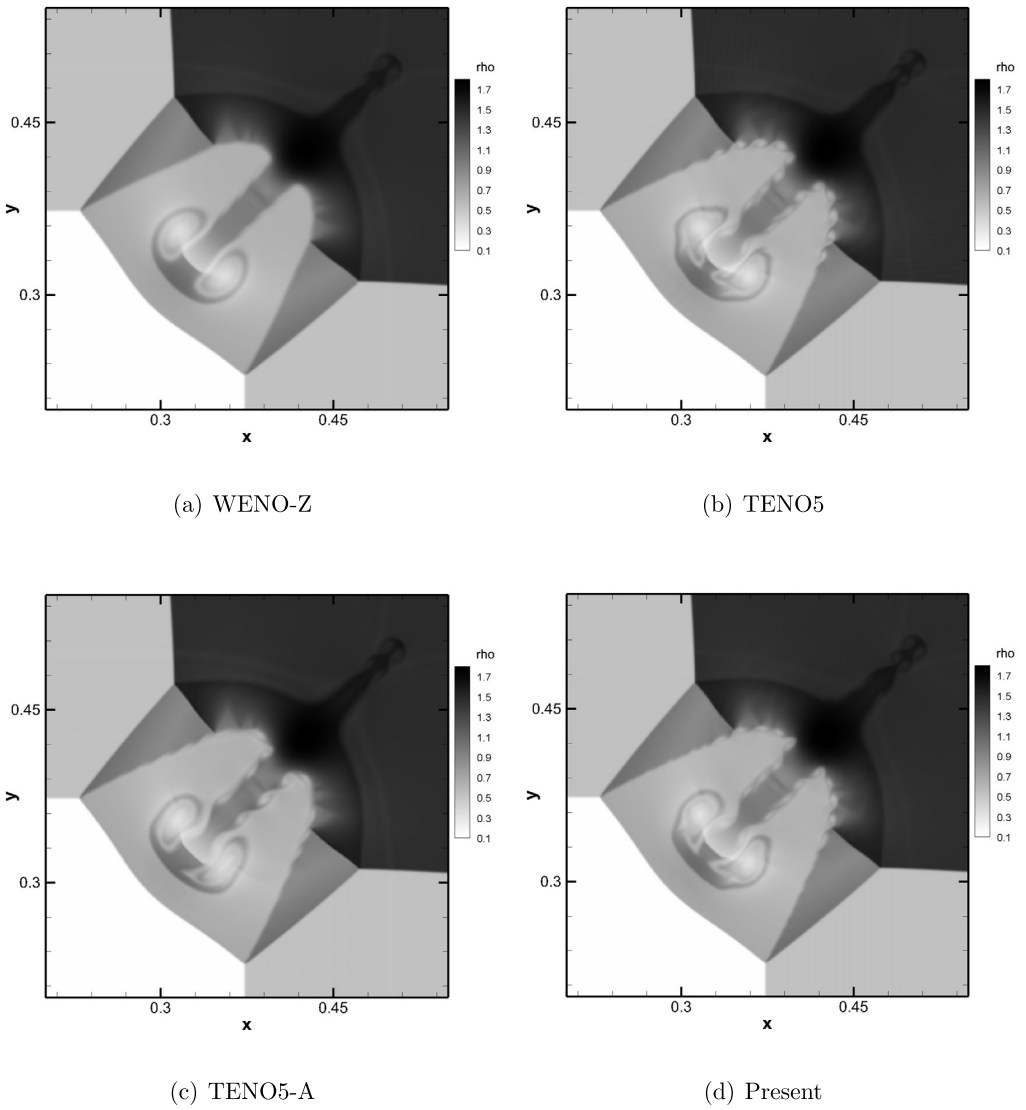

(a) WENO-Z (b) TENO5

(c) TENO5-A (d) Present

Fig. 15. Density contours for 2D Riemann problem with initial conditions Eq. (40).

The second case corresponds to configuration 12 in [58] with the initial conditions

$$(\rho, u, v, p) = \begin{cases} (0.8,\ 0,\ 0,\ 1.0) & x \le 0.5,\ y \le 0.5, \\ (1.0,\ 0.7276,\ 0,\ 1.0) & x \le 0.5,\ y > 0.5, \\ (1.0,\ 0.0,\ 0.7276,\ 1.0) & x > 0.5,\ y \le 0.5, \\ (0.5313,\ 0.0,\ 0.0,\ 0.4) & x > 0.5,\ y > 0.5. \end{cases} \tag{41}$$

Solutions are integrated to $t = 0.25$. As the small structures induced by the KH instability for this case require even lower dissipation and smaller grid size [41], a gird of (1400×1400) is used to illustrate the advantage of the presented method.

Density contours are shown in Fig. 17. The TENO schemes better resolve the small structures than WENOZ. The presented method resolves more small structures than the other schemes. Results of the TENO schemes computed with optimized weights are shown in Fig. 18. TENO5-A has a higher resolution of the structures than TENO5. The presented method obtains a similar resolution of the structures as TENO5-A.

4.3.3. Double Mach reflection

The double Mach reflection test is a mimic of the planar shock reflection in the air from wedges. It is a widely used benchmark to test the ability of shock capturing as well as the small scale structure resolution of a certain scheme. In the present simulation, the computation domain is taken as $[0, 4] \times [0, 1]$. The lower boundary is set to be a reflecting wall

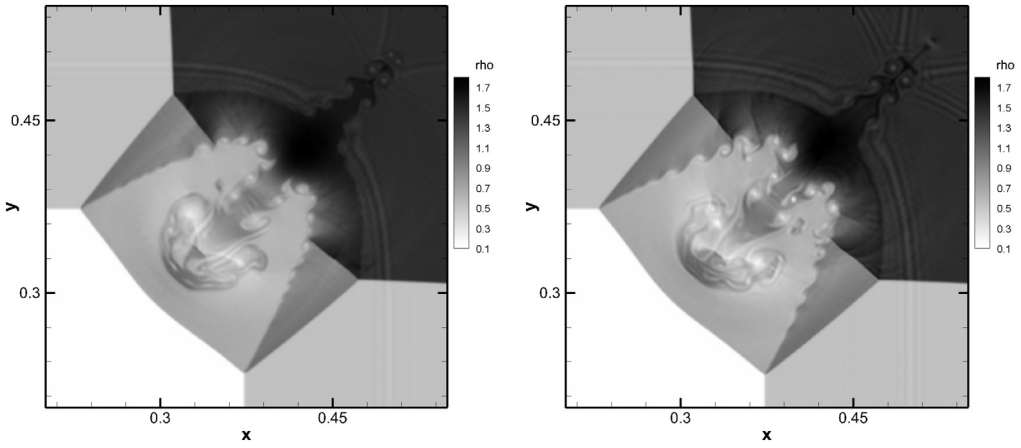

(a) TENO5 (b) TENO5-A

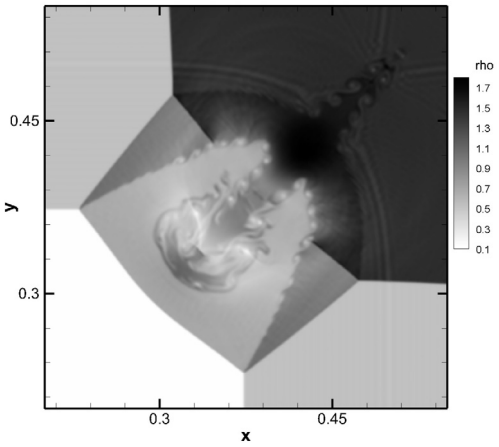

(c) Present

Fig. 16. Density contours for 2D Riemann problem with initial conditions Eq. (40), computed with optimized sub-stencil weights.

starting from $x = \frac{1}{6}$. At $t = 0$, a right-moving 60° inclined Mach 10 shock is positioned at $(\frac{1}{6}, 0)$. The upper boundary is set to describe the exact motion of the Mach 10 shock. The left boundary at $x = 0$ is assigned with post-shock values. Zero gradient outflow condition is set at $x = 4$. Readers may refer to [56,59] for detailed descriptions of the double Mach reflection problem. A uniform grid is used with $\Delta x = \Delta y = \frac{1}{256}$.

Fig. 19 shows the density contours of different methods at $t = 0.2$. All methods capture the discontinuities. Density contours of the roll-up region of different methods are shown in Figs. 20 to 23. Compared to the other schemes, the presented method resolves the K-H instability structures with lower dissipation.

In order to test the CFL effect on different schemes, numerical results with different CFL numbers are provided in Fig. 22 (CFL=0.4) and Fig. 23 (CFL=0.6). It can be seen that the resolved K-H structures are sensitive to the CFL number. TENO5-A varies more obviously than TENO5 and the present scheme. To test the performance of a spatial scheme, it seems reasonable to use a small CFL number.

4.3.4. High Mach number astrophysical jet

Consider the Mach 80 astrophysical jet problem [60,47]. This case is generally computed with the help of positivity-preserving methods. However, in this simulation, we do not incorporate such methods to evaluate the robustness of the tested schemes. The computational domain is $[0, 2] \times [-0.5, 0.5]$. The initial condition is given by:

$$(\rho, u, p) = (5.0, 0.0, 0.4127).$$

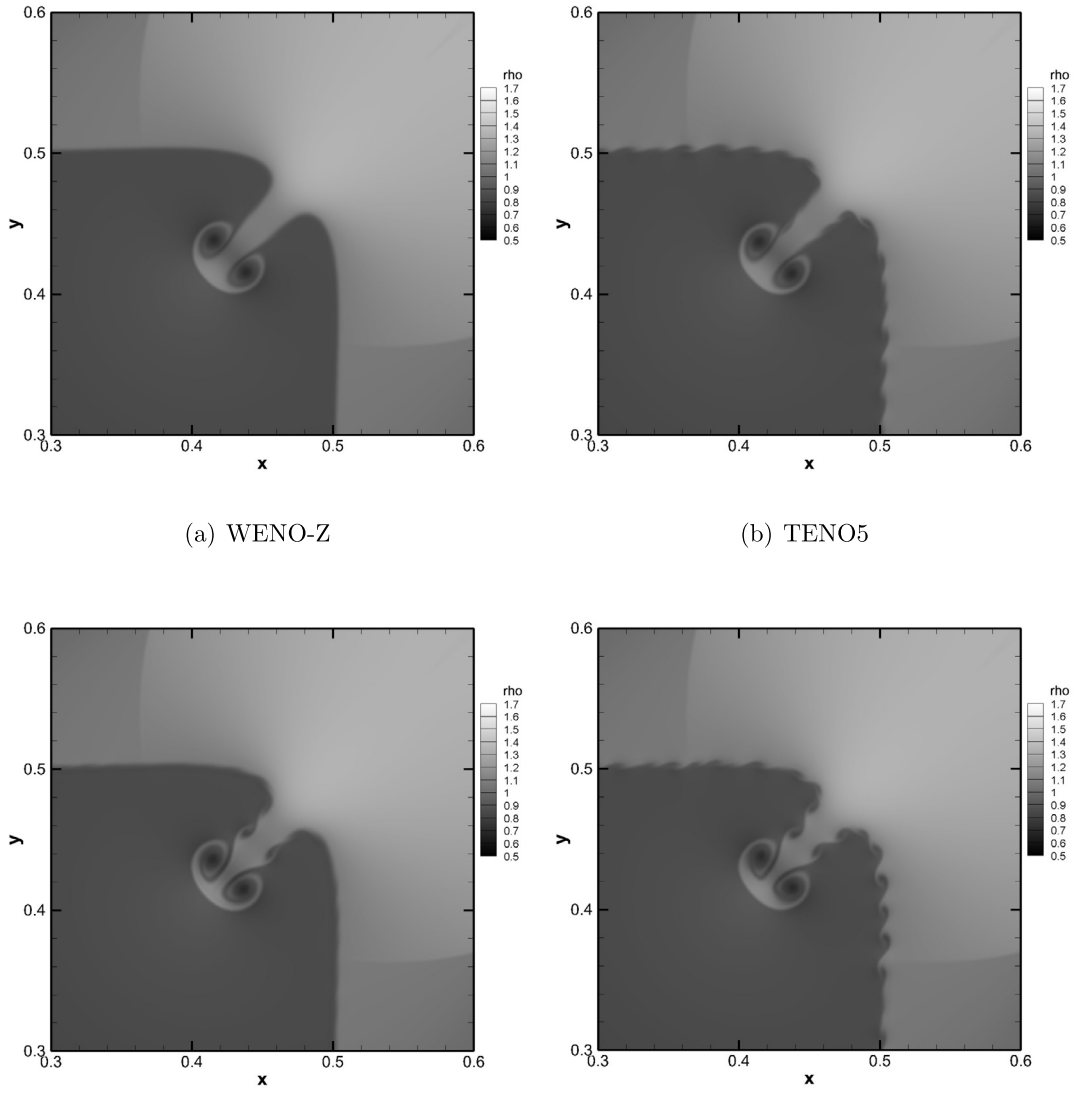

(a) WENO-Z (b) TENO5

(c) TENO5-A (d) Present

Fig. 17. Density contours for 2D Riemann problem with initial conditions Eq. (41) on a grid of 1400×1400.

For the left boundary if $y \in [-0.05, 0.05]$, then $(\rho, u, p) = (5.0, 30.0, 0.4127)$ otherwise $(\rho, u, p) = (5.0, 0.0, 0.4127)$. The boundary conditions for the top, bottom, and the right boundaries are outflow. γ is set to be $5/3$. The final time is 0.07.

Without the help of positivity-preserving methods, the parameters of the TENO schemes are adjusted to avoid failure. The parameter of TENO5 is set to be:

$$C_T = 10^{-2}.$$

The parameters of TENO5-A are set as:

$$a_1 = 10, \quad a_2 = 8, \quad C_r = 0.55, \quad \xi = 10^{-3}.$$

The parameters of TENO5-LAD are set as:

$$B_l = 2, \quad B_u = 10, \quad H = 1.57.$$

It should be noted that the parameters for TENO5-A and TENO5-LAD are obtained by fixing the upper and lower C_T bounds and fine-tuning the free parameters C_r and H for the best result of each scheme. The computation is performed on a $(N_x, N_y) = (512, 256)$ mesh. The CFL number for this simulation is 0.05 for all tested schemes.

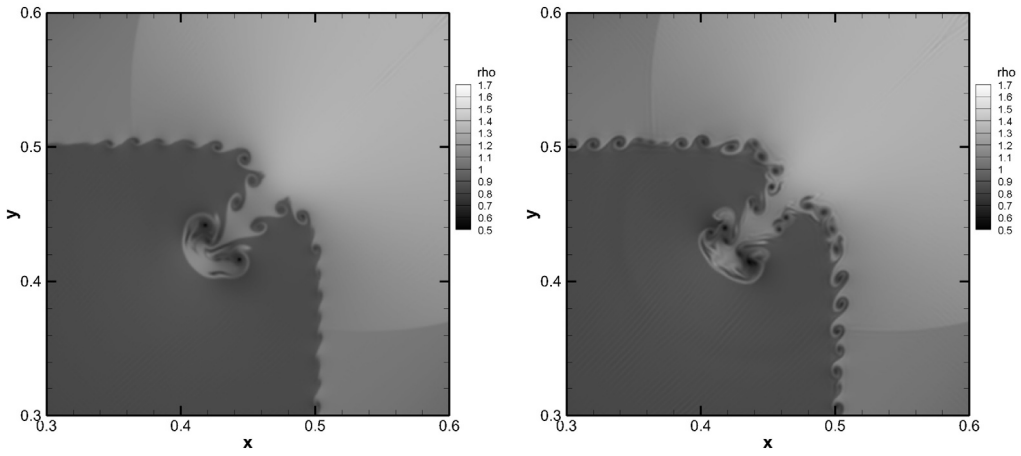

(a) TENO5 (b) TENO5-A

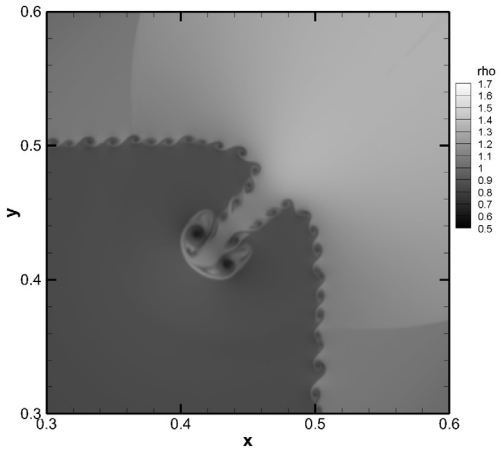

(c) Present

Fig. 18. Density contours for 2D Riemann problem with initial conditions Eq. (41) on a grid of 1400×1400, computed with optimized sub-stencil weights.

Table 2
Averaged computational time (in second) of a single time step of each scheme for different 2D cases, normalized values with respect to the computational time of TENO5 are given in the brackets.

Case	Grid number	WENO-Z	TENO5	TENO5-A	Present
Rayleigh–Taylor instability	128×512	0.14(0.93)	0.15(1.0)	0.2(1.33)	0.16(1.07)
	256×1024	0.59(0.88)	0.67(1.0)	0.88(1.31)	0.70(1.04)
2D Riemann Problem Case 1	1024×1024	2.57(0.88)	2.89(1.0)	3.71(1.28)	2.99(1.03)
2D Riemann Problem Case 2	1400×1400	5.03(0.88)	5.71(1.0)	8.26(1.45)	6.33(1.11)
Double Mach Reflection	1024×256	0.59(0.89)	0.66(1.0)	0.87(1.31)	0.69(1.05)
High Mach number jet	512×256	0.31(0.88)	0.35(1.0)	0.51(1.46)	0.38(1.08)

Fig. 24 shows the density contours of different methods at $t = 0.07$. Compared to the other schemes, the presented method better resolves the flow structures, especially the structures near the jet front.

4.3.5. Computational efficiency

The computational times of each scheme for different 2D cases are given in Table 2. All tests are computed on the same desktop workstation. TENO5-LAD needs about $5\% \sim 10\%$ more time than TENO5 while TENO5-A needs about $30\% \sim 40\%$ more computational time.

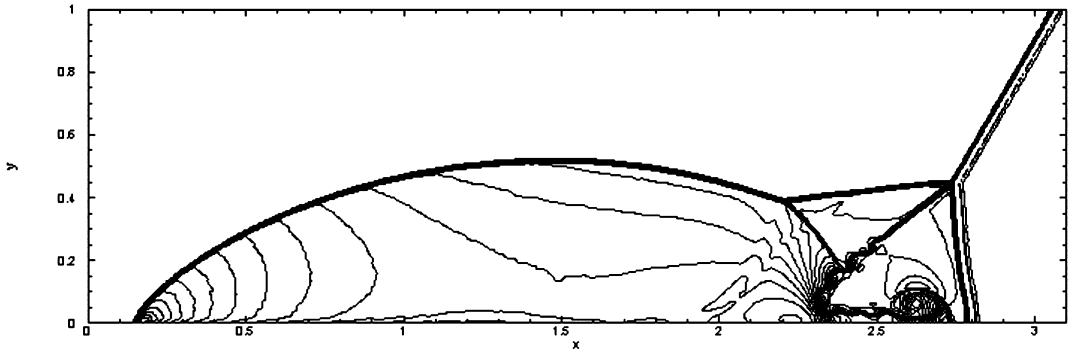

(a) WENO-Z

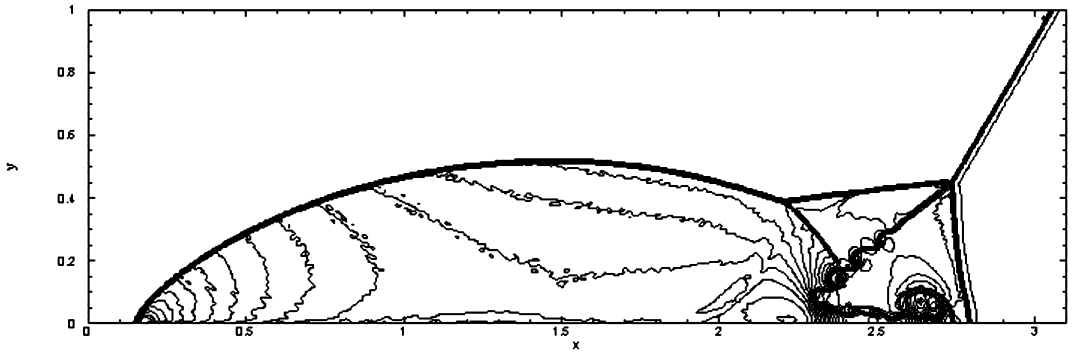

(b) TENO5

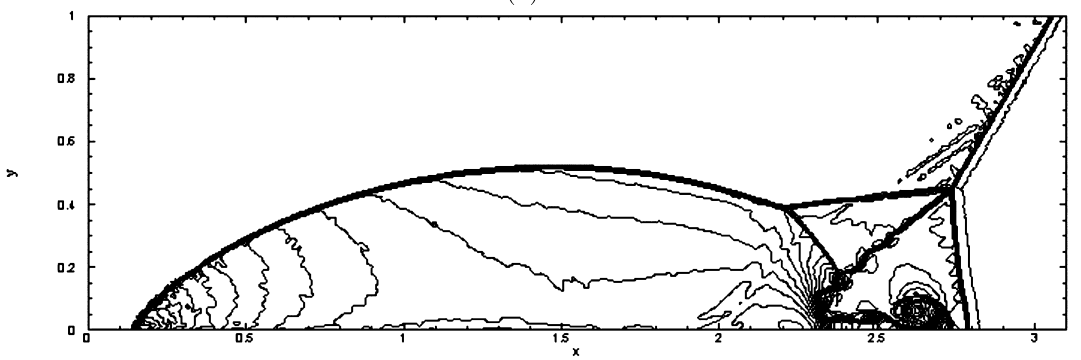

(c) TENO5-A

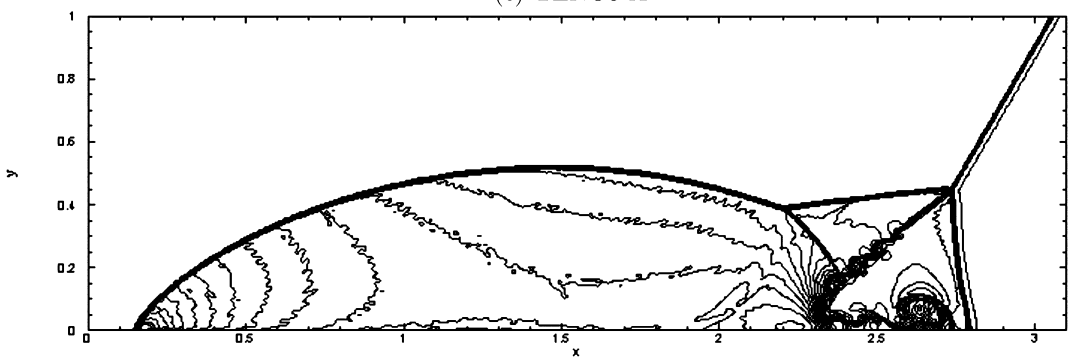

(d) Present

Fig. 19. Density contours of the double Mach reflection problem, ranging from $\rho = 1.4$ to 21 with 45 equally separated levels.

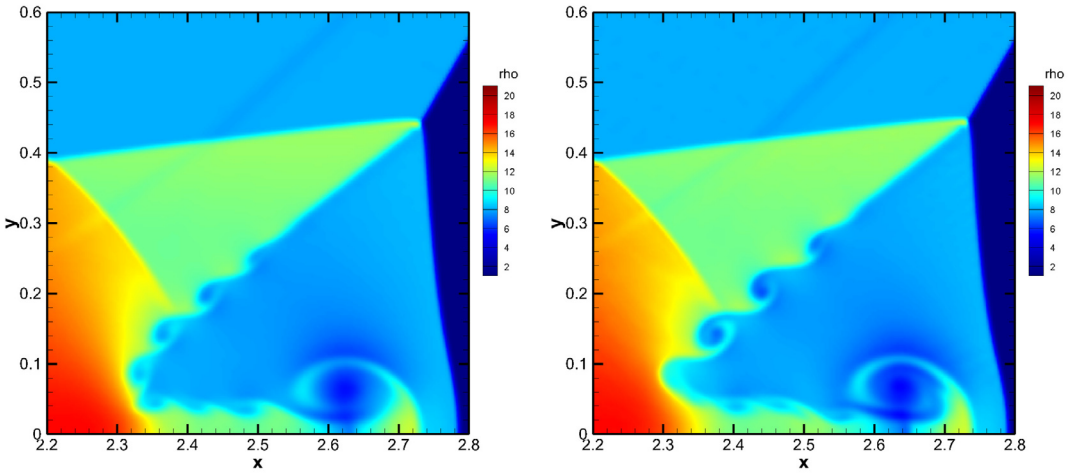

(a) WENO-Z (b) TENO5

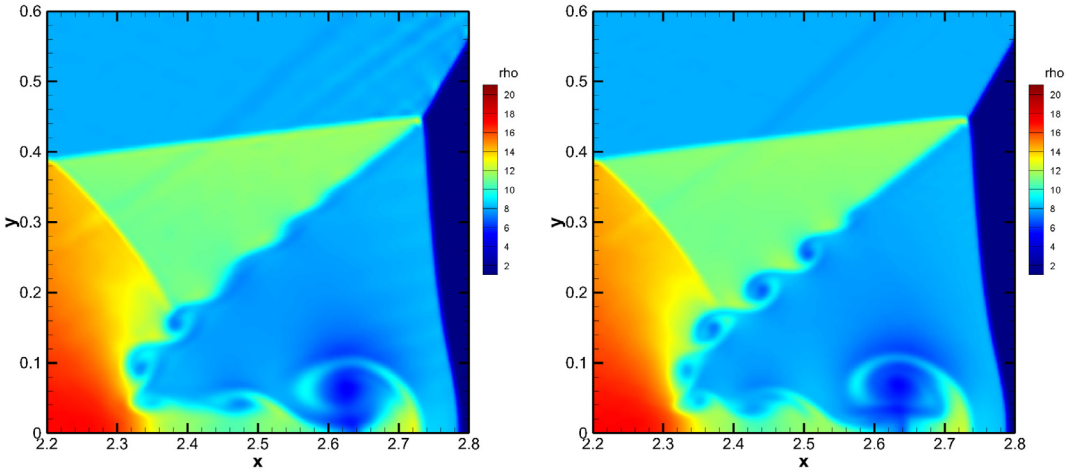

(c) TENO5-A (d) Present

Fig. 20. Zoom-in view of the roll-up region. (For interpretation of the colors in the figure(s), the reader is referred to the web version of this article.)

5. Conclusion

In this paper, an efficient target ENO scheme, the TENO5-LAD scheme, is proposed for compressible flow simulation. By utilizing a novel adaptive method, the cutoff parameter C_T is dynamically adjusted according to the smoothness of the reconstruction stencil. Numerical results show that the presented method maintains both of the ENO property and the low dissipation property of the TENO scheme at a lower extra computational cost. Due to the novel adaptive method, the presented method is more efficient than the TENO5 scheme and the TENO5-A scheme, and the pre-chosen value of the parameters can be applied to a wide range of cases. Furthermore, as only the most essential ingredients of TENO are required for the adaptive process, the presented method can be directly extended to higher-order TENO schemes.

CRediT authorship contribution statement

Jun Peng: Conceptualization, Methodology, Software, Writing - original draft. **Shengping Liu:** Software, Validation. **Shiyao Li:** Software, Validation, Visualization. **Ke Zhang:** Formal analysis, Validation, Visualization. **Yiqing Shen:** Funding acquisition, Supervision, Validation, Writing - review & editing.

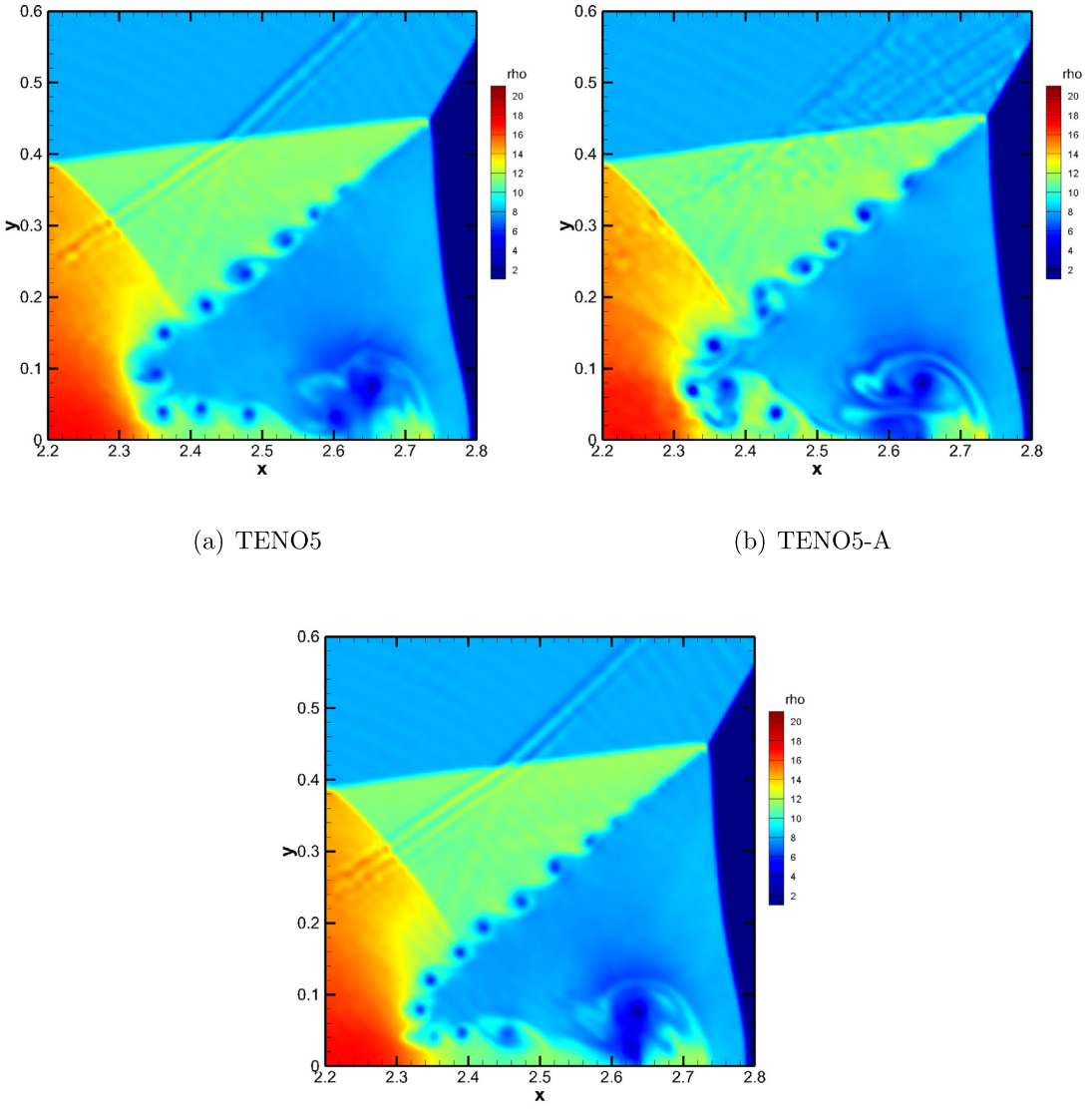

(a) TENO5

(b) TENO5-A

(c) Present

Fig. 21. Zoom-in view of the roll-up region computed with optimized sub-stencil weights. (For interpretation of the colors in the figure(s), the reader is referred to the web version of this article.)

Declaration of competing interest

The authors declare that they have no known competing financial interests or personal relationships that could have appeared to influence the work reported in this paper.

Acknowledgement

This paper is supported by the National Numerical Windtunnel project (NNW2019ZT1-A02). The first author is partially supported by NSFC under Grant No. 11902326 and the LHD Youth Innovation Fund under Grant No. LHD2019CX05. The fifth author is partially supported by NSFC under Grants Nos. 11872067 and 91852203 and NKRDPC No. 2016YFA0401200.

The authors acknowledge the anonymous reviewers for their valuable comments and suggestions. The authors also acknowledge Dr. Zhiwei He for his suggestions on the numerical examples.

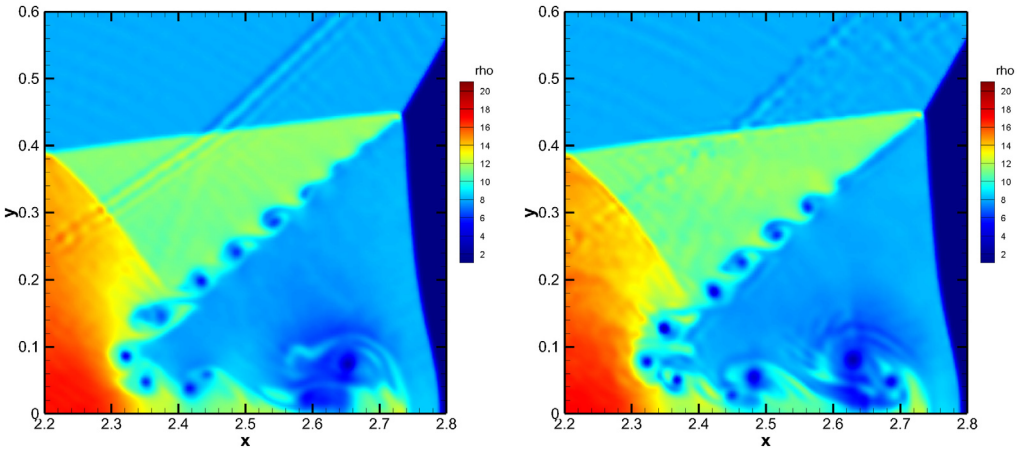

(a) TENO5 (b) TENO5-A

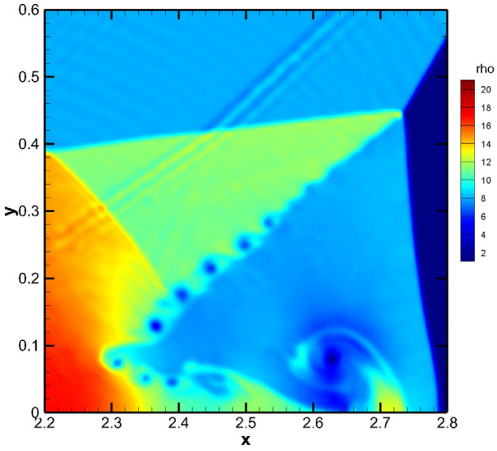

(c) Present

Fig. 22. Zoom-in view of the roll-up region computed with optimized sub-stencil weights, CFL=0.4. (For interpretation of the colors in the figure(s), the reader is referred to the web version of this article.)

References

[1] A. Harten, High resolution schemes for hyperbolic conservation laws, J. Comput. Phys. 49 (3) (1983) 357–393.
[2] A. Harten, B. Engquist, S. Osher, S.R. Chakravarthy, Uniformly high order accurate essentially non-oscillatory schemes, III, J. Comput. Phys. 71 (2) (1987) 231–303.
[3] S. Pirozzoli, Numerical methods for high-speed flows, Annu. Rev. Fluid Mech. 43 (1) (2011) 163–194.
[4] X.-D. Liu, S. Osher, T. Chan, Weighted essentially non-oscillatory schemes, J. Comput. Phys. 115 (1) (1994) 200–212.
[5] G.-S. Jiang, C.-W. Shu, Efficient implementation of weighted ENO schemes, J. Comput. Phys. 126 (1) (1996) 202–228.
[6] A.K. Henrick, T.A. Aslam, J.M. Powers, Mapped weighted essentially non-oscillatory schemes: achieving optimal order near critical points, J. Comput. Phys. 207 (2) (2005) 542–567.
[7] R. Borges, M. Carmona, B. Costa, W.S. Don, An improved weighted essentially non-oscillatory scheme for hyperbolic conservation laws, J. Comput. Phys. 227 (6) (2008) 3191–3211.
[8] M. Castro, B. Costa, W.S. Don, High order weighted essentially non-oscillatory WENO-Z schemes for hyperbolic conservation laws, J. Comput. Phys. 230 (5) (2011) 1766–1792.
[9] W.-S. Don, R. Borges, Accuracy of the weighted essentially non-oscillatory conservative finite difference schemes, J. Comput. Phys. 250 (2013) 347–372.
[10] N.K. Yamaleev, M.H. Carpenter, A systematic methodology for constructing high-order energy stable WENO schemes, J. Comput. Phys. 228 (11) (2009) 4248–4272.
[11] N.K. Yamaleev, M.H. Carpenter, Third-order energy stable WENO scheme, J. Comput. Phys. 228 (8) (2009) 3025–3047.
[12] P. Fan, Y. Shen, B. Tian, C. Yang, A new smoothness indicator for improving the weighted essentially non-oscillatory scheme, J. Comput. Phys. 269 (C) (2014) 329–354.
[13] S. Liu, Y. Shen, F. Zeng, M. Yu, A new weighting method for improving the WENO-Z scheme, Int. J. Numer. Methods Fluids 87 (6) (2018) 271–291.

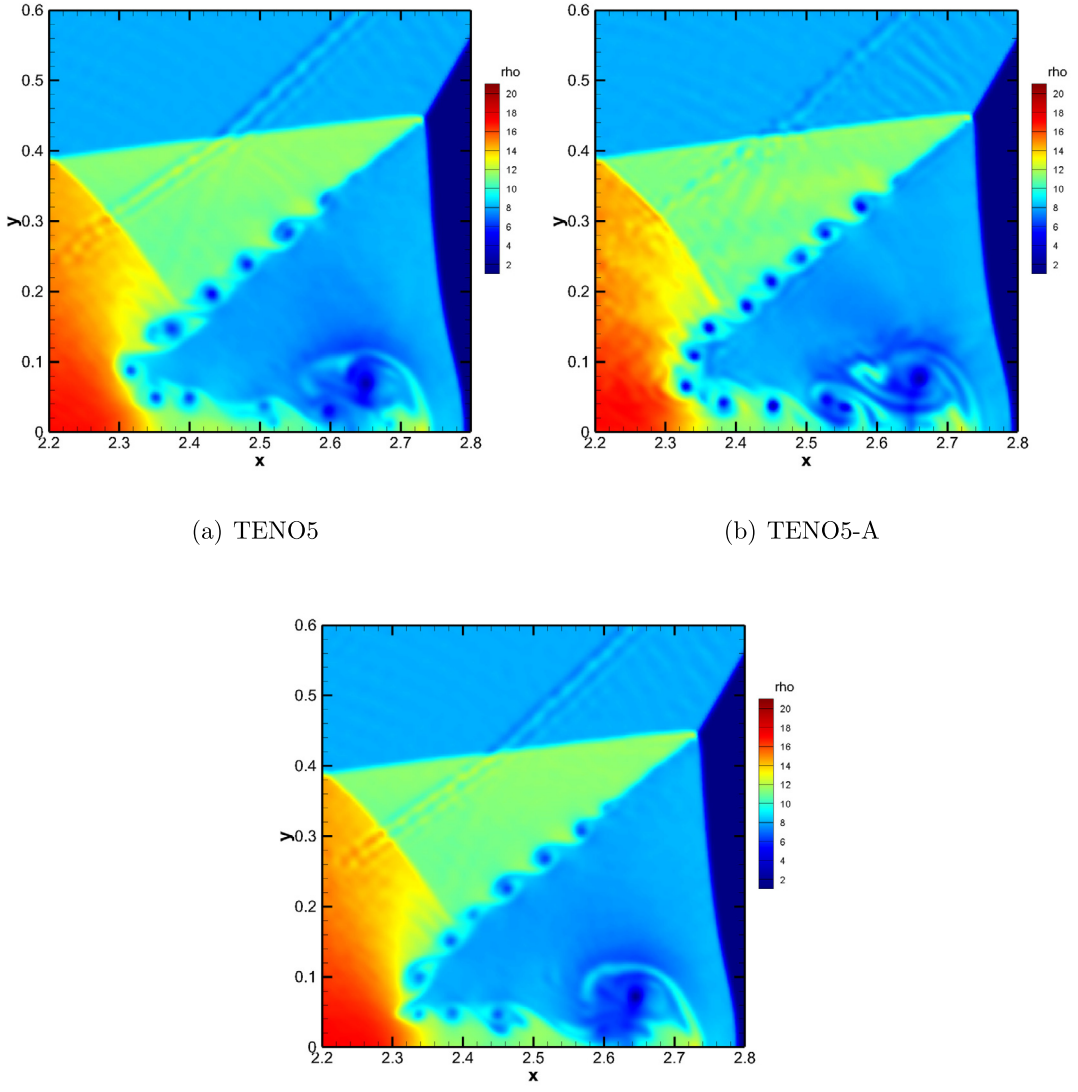

Fig. 23. Zoom-in view of the roll-up region computed with optimized sub-stencil weights, CFL=0.6. (For interpretation of the colors in the figure(s), the reader is referred to the web version of this article.)

[14] Y. Shen, G. Zha, Improvement of weighted essentially non-oscillatory schemes near discontinuities, Comput. Fluids 96 (C) (2014) 1–9.
[15] Y. Shen, L. Liu, Y. Yang, Multistep weighted essentially non-oscillatory scheme, Int. J. Numer. Methods Fluids 75 (4) (2014) 231–249.
[16] J. Peng, Y. Shen, Improvement of weighted compact scheme with multi-step strategy for supersonic compressible flow, Comput. Fluids 115 (2015) 243–255.
[17] Y. Ma, Z. Yan, H. Zhu, Improvement of multistep WENO scheme and its extension to higher orders of accuracy, Int. J. Numer. Methods Fluids 82 (12) (2016) 818–838.
[18] F. Zeng, Y. Shen, S. Liu, L. Liu, A high performance fifth-order multistep WENO scheme, Int. J. Numer. Methods Fluids 91 (4) (2019) 159–182.
[19] J. Zhu, J. Qiu, A new fifth order finite difference WENO scheme for solving hyperbolic conservation laws, J. Comput. Phys. 318 (2016) 110–121.
[20] J. Qiu, C.W. Shu, Hermite WENO schemes and their application as limiters for Runge-Kutta discontinuous Galerkin method: one-dimensional case, J. Comput. Phys. 193 (1) (2004) 115–135.
[21] J. Qiu, C.W. Shu, Hermite WENO schemes and their application as limiters for Runge-Kutta discontinuous Galerkin method II: two dimensional case, Comput. Fluids 34 (6) (2005) 642–663.
[22] Z. He, Y. Zhang, X. Li, L. Li, B. Tian, Preventing numerical oscillations in the flux-split based finite difference method for compressible flows with discontinuities, J. Comput. Phys. 300 (2015) 269–287.
[23] D. Levy, G. Puppo, G. Russo, Central WENO schemes for hyperbolic systems of conservation laws, ESAIM Math. Model. Numer. Anal. 33 (3) (1999) 547–571.
[24] I. Cravero, G. Puppo, M. Semplice, G. Visconti, Cweno: uniformly accurate reconstructions for balance laws, Math. Comput. 87 (312) (2018) 1689–1719.
[25] I. Cravero, G. Puppo, M. Semplice, G. Visconti, Cool WENO schemes, Comput. Fluids (2017).

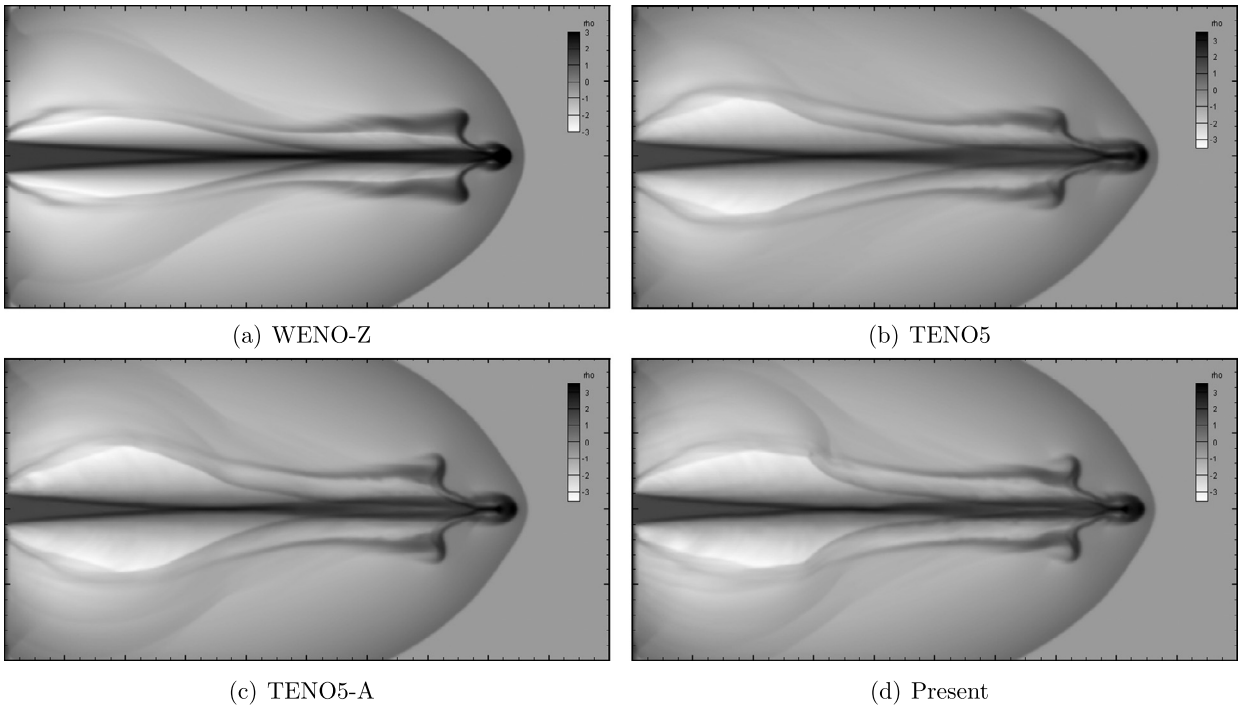

Fig. 24. Logarithmic density contours of the Mach 80 astrophysical jet problem, t=0.07.

[26] M.P. Martin, E.M. Taylor, M. Wu, V.G. Weirs, A bandwidth-optimized WENO scheme for the effective direct numerical simulation of compressible turbulence, J. Comput. Phys. 220 (1) (2006) 270–289.
[27] X.Y. Hu, Q. Wang, N.A. Adams, An adaptive central-upwind weighted essentially non-oscillatory scheme, J. Comput. Phys. 229 (23) (2010) 8952–8965.
[28] D.S. Balsara, C.W. Shu, Monotonicity preserving weighted essentially non-oscillatory schemes with increasingly high order of accuracy, J. Comput. Phys. 160 (2) (2000) 405–452.
[29] G.A. Gerolymos, D. Sénéchal, I. Vallet, Very-high-order WENO schemes, J. Comput. Phys. 228 (23) (2009) 8481–8524.
[30] S. Pirozzoli, On the spectral properties of shock-capturing schemes, J. Comput. Phys. 219 (2) (2006) 489–497.
[31] E. Johnsen, J. Larsson, A.V. Bhagatwala, W.H. Cabot, P. Moin, B.J. Olson, P.S. Rawat, S.K. Shankar, B. Sjögreen, H. Yee, et al., Assessment of high-resolution methods for numerical simulations of compressible turbulence with shock waves, J. Comput. Phys. 229 (4) (2010) 1213–1237.
[32] N.A. Adams, K. Shariff, A high-resolution hybrid compact-ENO scheme for shock-turbulence interaction problems, J. Comput. Phys. 127 (1) (1996) 27–51.
[33] S. Pirozzoli, Conservative hybrid compact-WENO schemes for shock-turbulence interaction, J. Comput. Phys. 178 (1) (2002) 81–117.
[34] D.J. Hill, D.I. Pullin, Hybrid tuned center-difference-WENO method for large eddy simulations in the presence of strong shocks, J. Comput. Phys. 194 (2) (2004) 435–450.
[35] B. Costa, W.S. Don, Multi-domain hybrid spectral-WENO methods for hyperbolic conservation laws, J. Comput. Phys. 224 (2) (2007) 970–991.
[36] S.K. Lele, Compact finite difference schemes with spectral-like resolution, J. Comput. Phys. 103 (1) (1992) 16–42.
[37] G.-Y. Zhao, M.-B. Sun, S. Pirozzoli, On shock sensors for hybrid compact/WENO schemes, Comput. Fluids (2020) 104439.
[38] G. Li, J. Qiu, Hybrid weighted essentially non-oscillatory schemes with different indicators, J. Comput. Phys. 229 (21) (2010) 8105–8129.
[39] J.L. Ziegler, R. Deiterding, J.E. Shepherd, D.I. Pullin, An adaptive high-order hybrid scheme for compressive, viscous flows with detailed chemistry, J. Comput. Phys. 230 (20) (2011) 7598–7630.
[40] Z. Gao, W.S. Don, Mapped hybrid central-WENO finite difference scheme for detonation waves simulations, J. Sci. Comput. 55 (2) (2012) 351–371.
[41] X. Deng, Y. Shimizu, F. Xiao, A fifth-order shock capturing scheme with two-stage boundary variation diminishing algorithm, J. Comput. Phys. 386 (2019) 323–349.
[42] Z. Sun, S. Inaba, F. Xiao, Boundary Variation Diminishing (BVD) reconstruction: a new approach to improve Godunov schemes, J. Comput. Phys. 322 (2016) 309–325.
[43] L. Fu, X.Y. Hu, N.A. Adams, A family of high-order targeted ENO schemes for compressible-fluid simulations, J. Comput. Phys. 305 (2016) 333–359.
[44] L. Fu, X.Y. Hu, N.A. Adams, Targeted ENO schemes with tailored resolution property for hyperbolic conservation laws, J. Comput. Phys. 349 (2017) 97–121.
[45] L. Fu, X.Y. Hu, N.A. Adams, A new class of adaptive high-order targeted ENO schemes for hyperbolic conservation laws, J. Comput. Phys. 374 (2018) 724–751.
[46] X.Y. Hu, N.A. Adams, Scale separation for implicit large eddy simulation, J. Comput. Phys. 230 (19) (2011) 7240–7249.
[47] L. Fu, A very-high-order TENO scheme for all-speed gas dynamics and turbulence, Comput. Phys. Commun. 244 (2019) 117–131.
[48] F. Zhang, J. Liu, H. Zhang, C. Xu, An extending strategy based on TENO framework for hyperbolic conservation laws, arXiv:1808.00037, 2018.
[49] L. Fu, X.Y. Hu, N.A. Adams, Improved five- and six-point targeted essentially nonoscillatory schemes with adaptive dissipation, AIAA J. 57 (3) (2019) 1143–1158.
[50] Y. Shen, G. Zha, Generalized finite compact difference scheme for shock/complex flowfield interaction, J. Comput. Phys. 230 (12) (2011) 4419–4436.
[51] J. Peng, Y. Shen, A novel weighting switch function for uniformly high-order hybrid shock-capturing schemes, Int. J. Numer. Methods Fluids 83 (9) (2017) 681–703.
[52] J. Peng, C. Zhai, G. Ni, H. Yong, Y. Shen, An adaptive characteristic-wise reconstruction WENO-Z scheme for gas dynamic Euler equations, Comput. Fluids 179 (2019) 34–51.

[53] C.-W. Shu, Total-variation-diminishing time discretizations, SIAM J. Sci. Stat. Comput. 9 (6) (1988) 1073–1084.
[54] P.D. Lax, Weak solutions of nonlinear hyperbolic equations and their numerical computation, Commun. Pure Appl. Math. 7 (1) (1954) 159–193.
[55] Y.-X. Ren, M. Liu, H. Zhang, A characteristic-wise hybrid compact-WENO scheme for solving hyperbolic conservation laws, J. Comput. Phys. 192 (2) (2003) 365–386.
[56] P. Woodward, P. Colella, The numerical simulation of two-dimensional fluid flow with strong shocks, J. Comput. Phys. 54 (1) (1984) 115–173.
[57] X. Zhang, C.W. Shu, Positivity-preserving high order finite difference WENO schemes for compressible Euler equations, J. Comput. Phys. 231 (5) (2012) 2245–2258.
[58] A. Kurganov, E. Tadmor, Solution of two-dimensional Riemann problems for gas dynamics without Riemann problem solvers, Numer. Methods Partial Differ. Equ. 18 (2002) 584–608.
[59] F. Kemm, On the proper setup of the double Mach reflection as a test case for the resolution of gas dynamics codes, Comput. Fluids 132 (2016) 72–75.
[60] X. Zhang, C.W. Shu, On positivity-preserving high order discontinuous Galerkin schemes for compressible Euler equations on rectangular meshes, J. Comput. Phys. 229 (23) (2010) 8918–8934.